

PREPARED FOR SUBMISSION TO JHEP

Generalized Volume-Complexity For Two-Sided Hyperscaling Violating Black Branes

Farzad Omidi

*School of Physics, Institute for Research in Fundamental Sciences (IPM),
P.O. Box 19395-5531, Tehran, Iran*

E-mail: farzad@ipm.ir

ABSTRACT: In this paper, we investigate generalized volume-complexity \mathcal{C}_{gen} for a two-sided uncharged HV black brane in $d + 2$ dimensions. This quantity which was recently introduced in [48], is an extension of volume in the Complexity=Volume (CV) proposal, by adding higher curvature corrections with a coupling constant λ to the volume functional. We numerically calculate the growth rate of \mathcal{C}_{gen} for different values of the hyperscaling violation exponent θ and dynamical exponent z . It is observed that \mathcal{C}_{gen} always grows linearly at late times provided that we choose λ properly. Moreover, it approaches its late time value from below. For the case $\lambda = 0$, we find an analytic expression for the late time growth rate for arbitrary values of θ and z . However, for $\lambda \neq 0$, the late time growth rate can only be calculated analytically for some specific values of θ and z . We also examine the dependence of the growth rate on d , θ , z and λ . Furthermore, we calculate the complexity of formation obtained from volume-complexity and show that it is not UV divergent. We also examine its dependence on the thermal entropy and temperature of the black brane. At the end, we also numerically calculate the growth rate of \mathcal{C}_{gen} for the case where the higher curvature corrections are a linear combination of the Ricci scalar, square of the Ricci tensor and square of the Riemann tensor. We show that for appropriate values of the coupling constants, the late time growth rate is again linear.

KEYWORDS: AdS-CFT Correspondence, Gauge-gravity correspondence

ARXIV EPRINT: [2207.05287](https://arxiv.org/abs/2207.05287)

Contents

| | | |
|----------|--|-----------|
| 1 | Introduction | 1 |
| 2 | Hyperscaling Violating Black Brane | 4 |
| 3 | Generalized Volume-Complexity \mathcal{C}_{gen} | 6 |
| 3.1 | Growth Rate | 9 |
| 3.2 | $\lambda = 0$: Volume-Complexity | 11 |
| 3.2.1 | General Time Dependence | 12 |
| 3.3 | Maxima of the Effective Potential For $\lambda \neq 0$ | 12 |
| 3.3.1 | $\theta = 0$ | 15 |
| 3.3.2 | $\theta = 0$ and $z = 1$ | 19 |
| 3.3.3 | $d = 2$, $\theta = 1$ and $z = 1$ | 21 |
| 3.4 | General Time Dependence for $\lambda \neq 0$ and Arbitrary Values of θ and z | 21 |
| 4 | Complexity of Formation | 27 |
| 4.1 | $\theta = 0$ | 27 |
| 4.2 | $\theta \neq 0$ | 29 |
| 4.2.1 | $d_e \neq \theta_e$ | 29 |
| 4.2.2 | $d_e = \theta_e$ | 30 |
| 5 | Discussion | 31 |
| | Appendix | 32 |
| A | Connection between the Radial Cutoffs | 32 |
| A.1 | $\theta = 0$ | 33 |
| A.2 | $\theta \neq 0$ | 35 |
| B | Other Higher Derivative Functionals $F_{1,2}(g_{\mu\nu}; X^\mu(\sigma))$ | 37 |

1 Introduction

In the last two decades, we witnessed that quantum information quantities such as entanglement entropy and quantum complexity have been very fruitful in understanding the AdS/CFT correspondence (See [1–3] for a review). Quantum complexity is defined as the minimum number of simple unitary operations required to prepare a given state from an initial reference state [4]. One of the intriguing features of quantum complexity is that it continues to grow

long after the time at which entanglement entropy saturates [3, 5–9]. Therefore, it is widely believed that it can provide information about the interior of black holes. In the context of AdS/CFT [10], there are two main proposals for the calculation of quantum complexity: Complexity=Volume (CV) [6, 7] and Complexity=Action (CA) [8, 9]. It should be pointed out that volume-complexity¹ was also introduced for some subregions in the bulk spacetime such as in a region [11, 12] enclosed by a (H)RT hypersurface [13, 14] or inside a Wheeler-DeWitt (WDW) patch [15].² Various aspects of the CV and CA proposals have been explored extensively in the literature [16–51] such as: subregion complexity [52–67], complexity of formation [21, 68–70], in Jackiw-Teitelboim gravity [71–73], for higher derivative gravity [74–76], for Kerr-AdS black holes [69, 77], at finite radial cutoff [72, 78–82], structure of the UV divergent terms [62, 70, 83–85], regularization methods [70, 85] and covariant counterterms on spacelike/timelike [21, 70, 72, 78–82, 84–86] or null [21, 70, 84–86] boundaries or joint points [87] of the WDW patch. For a detailed review refer to [3]. Moreover, quantum complexity was also investigated from the QFT point of view [38, 39, 42, 88–126].

According to the CV proposal [6, 7], the complexity of a state on a constant time slice Σ_τ in a holographic CFT is given by the volume $V(\Sigma(\tau))$ of an extremal codimension-one hypersurface $\Sigma(\tau)$ in the bulk spacetime³

$$\mathcal{C}_V = \max_{\partial\Sigma(\tau)=\Sigma_\tau} \left[\frac{V(\Sigma(\tau))}{\ell G_N} \right] = \max_{\partial\Sigma(\tau)=\Sigma_\tau} \left[\frac{1}{G_N L} \int_{\Sigma(\tau)} d^{d+1} \sigma \sqrt{h} \right]. \quad (1.1)$$

Here $\Sigma(\tau)$ is anchored on the left and right asymptotic boundaries of the bulk spacetime at times t_L and t_R such that $\partial\Sigma(\tau) = \Sigma_\tau$ (See Figure 1). Moreover, h is the induced metric on $\Sigma(\tau)$ and ℓ is a dimensionful constant which can be either the AdS radius L or the black hole horizon radius r_h . In the following, we set $\ell = L$.

Recently, CV proposal was generalized in ref. [48] and the following functional was introduced as the holographic dual of quantum complexity

$$O_{F_1, \Sigma_{F_2}}(\Sigma_\tau) = \frac{1}{G_N L} \int_{\Sigma_{F_2}} d^{d+1} \sigma \sqrt{h} F_1(g_{\mu\nu}; X^\mu). \quad (1.2)$$

Here the integral is taken on a codimension-one hypersurface Σ_{F_2} in the bulk spacetime which is anchored on the boundary of the bulk spacetime such that $\partial\Sigma_{F_2} = \Sigma_\tau$ where Σ_τ is a constant time slice in the boundary where the dual CFT lives. Moreover, it is parametrized by the coordinates $X^\mu(\sigma^i)$ and σ^i are the coordinates in the bulk spacetime. $F_{1,2}(g_{\mu\nu}, X^\mu)$ are arbitrary scalar functions of the bulk metric $g_{\mu\nu}$ and $X^\mu(\sigma^i)$. Furthermore, h is the determinant of the induced metric on Σ_{F_2} , and the hypersurface Σ_{F_2} is determined by extremizing the following functional [48]

$$\delta_X \left(\int_{\Sigma_{F_2}} d^{d+1} \sigma \sqrt{h} F_2(g_{\mu\nu}; X^\mu) \right) = 0. \quad (1.3)$$

¹We call the holographic complexity in the CV proposal *volume-complexity*.

²This proposal is also called CV2.0.

³Here, we assume that the bulk spacetime is $d + 2$ dimensional.

Therefore, F_2 determines the hypersurface Σ_{F_2} on which the integral in eq. (1.2) is taken and F_1 determines $O_{F_1, \Sigma_{F_2}}$. It should be pointed out that F_1 and F_2 are two independent functions. However, for $F_1 = F_2$, eq. (1.2) can be simplified as follows

$$\mathcal{C}_{\text{gen}}(\tau) = \max_{\partial\Sigma(\tau)=\Sigma_\tau} \left[\frac{1}{G_{NL}} \int_{\Sigma(\tau)} d^{d+1} \sigma \sqrt{h} F_1(g_{\mu\nu}; X^\mu(\sigma)) \right], \quad (1.4)$$

where $\tau = 2t_L = 2t_R$ ⁴ and $t_{L,R}$ are the time coordinates in the left and right CFTs. Moreover, for $F_1 = F_2 = 1$, the functional in eq. (1.2) reduces to the volume functional in the CV proposal, i.e. eq. (1.1). Since \mathcal{C}_{gen} is a generalization of the volume-complexity, it is dubbed *generalized* volume-complexity. It should also be emphasize that the extremal hypersurface $\Sigma(\tau)$ approaches a constant- r hypersurface at $r = r_f$ at late times, i.e. $\tau \rightarrow \infty$, which is called the *final* slice [7, 48] (See Figure 1). Moreover, it was shown in ref. [48] that finding the extremal hypersurface $\Sigma(\tau)$ in eq. (1.4), is analogous to study the motion of a classical non-relativistic particle in an effective potential $\hat{U}(r)$ with the action $S \propto \mathcal{C}_{\text{gen}}$. In this manner, extremizing equations for \mathcal{C}_{gen} are equivalent to the equations of motion of the particle (See eqs. (3.7) and (3.8)).⁵ Furthermore, the growth rate of \mathcal{C}_{gen} behaves as follows [48]

$$\frac{d\mathcal{C}_{\text{gen}}}{d\tau} = \frac{1}{2} P_t |_{\partial\Sigma(t)}, \quad (1.5)$$

where P_t is the momentum conjugate to the time coordinate t . Therefore, to have a linear growth rate at late times, P_t has to be a constant at late times. It was also shown in ref. [48] that, it happens whenever the effective potential has a local maximum *inside* the horizon. Therefore, investigating the local maxima of $\hat{U}(r)$ is crucial.

The aim of the paper is to explore the generalized volume-complexity for a two-sided Hyper-scaling Violating (HV) black brane [127] in $d + 2$ dimensions. Different aspects of this background have been studied in the literature such as: Page curve [128], Volume-Complexity [23]⁶ and Action-Complexity [23, 24, 81]. Similar to ref. [48], we consider the following case

$$F_1(g_{\mu\nu}; X^\mu(\sigma)) = F_2(g_{\mu\nu}; X^\mu(\sigma)) = 1 + \lambda L^4 C^2, \quad (1.6)$$

where $C^2 = C_{\alpha\beta\mu\nu} C^{\alpha\beta\mu\nu}$ is the square of the Weyl tensor in the bulk and L is a length scale which reduces to the AdS radius when $\theta = 0$ and $z = 1$. Moreover, λ is a dimensionless coupling constant and it can have any value. However, we will see that asking for \mathcal{C}_{gen} to have a linear growth at late times, imposes a constraint on the value of λ . We calculate generalized volume-complexity for the two cases $\lambda = 0$ and $\lambda \neq 0$, separately. For both cases, we numerically obtain the growth rate of \mathcal{C}_{gen} . For $\lambda = 0$, we find analytically the growth

⁴In the following, we consider symmetric hypersurfaces Σ_τ for which $t_L = t_R$ (See Figure 1). Since $\tau = t_L + t_R$, one has $\tau = 2t_L = 2t_R$

⁵The same prescription also works for volume-complexity (See e.g. ref. [21]).

⁶It should be emphasized that our HV black brane solution is connected to that investigated in ref. [23]. More precisely, by changing the radial coordinate as $r_{\text{there}} = \frac{L^2}{r_{\text{here}}^{\theta}} r_{\text{here}}^{\theta-1}$, the two solutions transform to each other. We would like to thank the referee for her/his helpful comments in this regard.

rate. However, for $\lambda \neq 0$, we can find it analytically for some specific cases: 1) $\theta = 0$ and arbitrary values of d and z , 2) $d = 2$, $\theta = 1$ and $z = 1$. We also prove that $\frac{d\mathcal{C}_{\text{gen}}}{d\tau}$ reaches its late time value from below similar to AdS black holes. Moreover, we write the growth rate in terms of the effective potential of a classical non-relativistic particle and investigate its maxima in detail. On the other hand, we calculate the complexity of formation $\Delta\mathcal{C}_V$ obtained from volume-complexity and show that it is a UV finite quantity. Furthermore, for $\theta = 0$, it is proportional to the thermal entropy S of the black brane. For $\theta \neq 0$, there are two cases $d_e \neq \theta_e$ and $d_e = \theta_e$ which have different kinds of UV divergent terms in \mathcal{C}_V , and hence have to be considered separately. For the former, $\Delta\mathcal{C}_V$ is proportional to $ST^{-\frac{\theta_e}{z}}$ where T is the temperature of the black brane. However, for the latter, it depends on $\log S$.

The outline of the paper is as follows: in Section 2, we briefly review HV black branes. In Section 3, we calculate generalized volume-complexity for this background. In Section 4, we calculate the complexity of formation $\Delta\mathcal{C}_V$ obtained from volume-complexity. In Section 5, we summarize our results and discuss about future problems. Moreover, in Appendix A, we investigate the connection between the radial cutoffs r_{max} of the black brane and vacuum. These results are necessary for the calculation of the complexity of formation. In Appendix B, we study the generalized complexity for the case where $F_1 = F_2$ such that they are an arbitrary combination of Ricci scalar, square of the Ricci tensor and square of the Riemann tensor.

2 Hyperscaling Violating Black Brane

In this section, we review Hyperscaling Violating (HV) black branes which are solutions to the Einstein-Maxwell-Dilaton gravity theory. The corresponding action is given by [127]

$$I_{\text{HV}} = -\frac{1}{16\pi G_N} \int d^{d+2}x \sqrt{-g} \left[R - \frac{1}{2} (\partial\phi)^2 + V(\phi) - \frac{1}{4} e^{\lambda\phi} F^2 \right]. \quad (2.1)$$

The scalar field ϕ , the potential $V(\phi)$ and the field strength of the gauge field are as follows [127]

$$\begin{aligned} \phi &= \phi_0 + \beta \ln r, \\ V(\phi) &= (d_e + z - 1)(d_e + z) e^{\gamma(\phi - \phi_0)}, \\ F_{rt} &= \sqrt{2(z-1)(d_e + z)} e^{\frac{(d_e + \theta_e)\phi_0}{\beta}} r^{d_e + z - 1}, \end{aligned} \quad (2.2)$$

where

$$\beta = \sqrt{2d_e(-\theta_e + z - 1)}, \quad \lambda = -\frac{2(d_e + \theta_e)}{\beta}, \quad \gamma = \frac{2\theta_e}{\beta}. \quad (2.3)$$

Moreover, $d_e = d - \theta$ is the effective dimension [129] and $\theta_e = \frac{\theta}{d}$. The metric is given by [127, 130]⁷

$$ds^2 = \left(\frac{r}{r_F}\right)^{-2\theta_e} \left(-\left(\frac{r}{L}\right)^{2z} f(r) dt^2 + \frac{L^2}{r^2 f(r)} dr^2 + \frac{r^2}{L^2} \sum_{i=1}^d dx_i^2 \right), \quad (2.4)$$

where

$$f(r) = 1 - \left(\frac{r_h}{r}\right)^{d_e+z}. \quad (2.5)$$

It should be emphasized that the solution has two parameters z and θ which are called the dynamical and hyperscaling violation exponents, respectively. Furthermore, under the following coordinate transformation [129]

$$t \rightarrow \lambda^z t \quad x^i \rightarrow \lambda x^i \quad r \rightarrow \lambda^{-1} r, \quad (2.6)$$

the metric (2.4) behaves as follows

$$ds \rightarrow \lambda^{\theta_e} ds, \quad (2.7)$$

and hence it is not invariant. However, for $\theta = 0$, the metric is scale invariant. Moreover, there is an anisotropy among the t and x^i directions in eq. (2.6). Therefore, the Lorentz symmetry is also broken for $z \neq 1$. In other words, for $\theta = 0$ and $z = 1$, the scaling and Lorentz symmetries are restored in the dual QFT. In this case, the solution reduces to a $d+2$ dimensional planar AdS-Schwarzschild black hole.⁸ Another important point is that the null energy condition imposes the following constraints on z and θ [129]

$$d_e(d(z-1) - \theta) \geq 0, \quad (z-1)(d_e+z) \geq 0. \quad (2.8)$$

Moreover, it was argued in ref. [127] that the solution is not valid for $d = \theta$. On the other hand, it was shown that the solution is not stable for $d < \theta$ [129]. Therefore, we restrict ourselves to the following cases

$$z \geq 1, \quad d > \theta. \quad (2.9)$$

On the other hand, the temperature and entropy of the black brane are given by [127, 130]

$$T = \frac{(d_e+z)r_h^z}{4\pi L^{z+1}}, \quad S = \frac{V_d r_h^{d_e} r_F^\theta}{4G_N L^d}. \quad (2.10)$$

⁷Notice that there are two dimensionful parameters r_F and r_f which have very similar notations. Here, r_F is the dynamical scale in the HV geometry and the metric in eq. (2.4) is only well-defined for $r > r_F$ [129, 131]. On the other hand, r_f is the radial coordinate of the final r-constant hypersurface that the extremal surface $\Sigma(\tau)$ approaches it at late times (See Figure 1).

⁸Notice that for $z = 1$, the gauge field is zero. Moreover, for $\theta = 0$, the scalar field becomes a constant. In this case, $V(\phi)$ plays the role of the cosmological constant.

Moreover, the mass is as follows [130]⁹

$$M = \frac{d_e}{d_e + z} TS = \frac{d_e V_d}{16\pi G_N} \frac{r_h^{d_e+z} r_F^\theta}{L^{d+z+1}}. \quad (2.11)$$

Furthermore, the tortoise coordinate is simply given by

$$r^*(r) = \int \frac{L^{z+1}}{r^{z+1} f(r)} dr, \quad (2.12)$$

which is a hypergeometric function of r [128]. However, we do not need the explicit form of $r^*(r)$ here. It should be pointed out that this theory has a vacuum solution which is obtained by setting $f(r) = 1$ in eq. (2.4) [129, 132]

$$ds^2 = \left(\frac{r}{r_F}\right)^{-2\theta_e} \left(- \left(\frac{r}{L}\right)^{2z} dt^2 + \frac{L^2}{r^2} dr^2 + \frac{r^2}{L^2} \sum_{i=1}^d dx_i^2 \right), \quad (2.13)$$

whose entropy and temperature are zero. In Section 4, we need the volume-complexity of the vacuum to calculate the complexity of formation.

3 Generalized Volume-Complexity \mathcal{C}_{gen}

To calculate the generalized volume-complexity in eq. (1.4), we proceed in the same manner as refs. [21, 48]. In the infalling Eddington-Finkelstein coordinate $v = t + r^*$, the metric in eq. (2.4) can be written as follows

$$ds^2 = \left(\frac{r}{r_F}\right)^{-2\theta_e} \left(- \left(\frac{r}{L}\right)^{2z} f(r) dv^2 + 2 \left(\frac{r}{L}\right)^{z-1} dv dr + \frac{r^2}{L^2} \sum_{i=1}^d dx_i^2 \right). \quad (3.1)$$

Due to the translational symmetry along the transverse directions $x^{i=1\dots d}$, we parametrize the spacelike hypersurface $\Sigma(\tau)$ as follows

$$\Sigma(\tau) : (v(\sigma), r(\sigma), \vec{x}). \quad (3.2)$$

As mentioned before, here we consider symmetric configurations for which one has $t_L = t_R$ (See Figure 1). Then one can write the generalized volume-complexity as follows

$$\mathcal{C}_{\text{gen}} = \frac{V_d}{G_N L} \int d\sigma \frac{r^{d_e - \theta_e}}{r_F^{-\theta_e(d+1)} L^d} \sqrt{- \left(\frac{r}{L}\right)^{2z} f(r) \dot{v}^2 + 2 \left(\frac{r}{L}\right)^{z-1} \dot{v} \dot{r} a(r)}, \quad (3.3)$$

⁹ In the literature, the metric of the transverse directions in eq. (2.4) is written as $d\Omega_d^2 = \frac{1}{L^2} \sum_{i=1}^d dx_i^2$. Notice that $\Omega_d = \frac{V_d}{L^d}$, where Ω_d and V_d are the volumes of the metrics $d\Omega_d^2$ and $\sum_{i=1}^d dx_i^2$, respectively. Having said this, the entropy and mass of a HV black brane can be written as $S = \frac{\Omega_d r_h^{d_e} r_F^\theta}{4G_N}$ and $M = \frac{d_e V_d}{16\pi G_N} \frac{r_h^{d_e+z} r_F^\theta}{L^{z+1}}$ [130]. It should also be pointed out that Ω_d is dimensionless and V_d has the dimension of length^d.

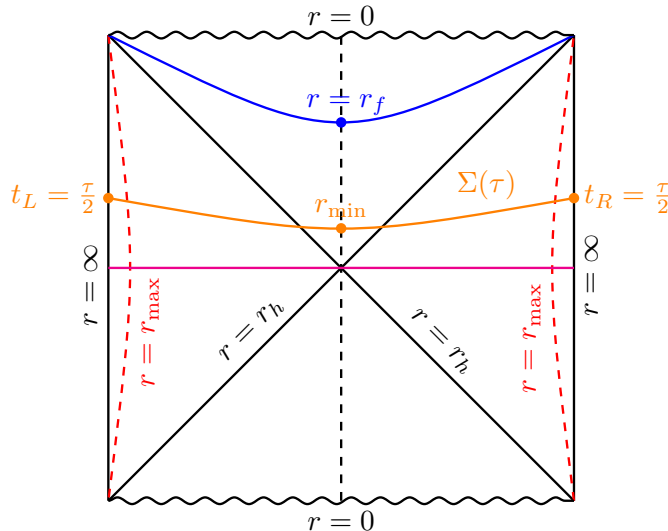


Figure 1. The extremal codimension-one bulk hypersurface $\Sigma(\tau)$ denoted in orange, starts from the left boundary at time t_L , then goes inside the horizon and reaches the minimal radius r_{\min} . Next, it goes outside the horizon and reaches the right asymptotic boundary at time t_R . Here, we consider symmetric hypersurfaces where $t_L = t_R = \frac{\tau}{2}$. At late times, i.e. $\tau \rightarrow \infty$, it approaches a constant- r hypersurface dubbed *final slice* at $r = r_f$ which is denoted in blue. The red dashed curves are the radial cutoffs at $r = r_{\max}$. Moreover, the magenta straight line denotes the extremal hypersurface anchored at $t_L = t_R = 0$ which is applied in the calculation of the complexity of formation in Section 4.

where

$$a(r) = 1 + \lambda L^4 C^2, \quad (3.4)$$

and λ is a *dimensionless* coupling constant. Moreover, “.” denotes the derivative with respect to the coordinate σ and V_d is the volume of the spatial directions $x^{i=1, \dots, d}$. Since \mathcal{C}_{gen} is invariant under the diffeomorphism $\sigma \rightarrow g(\sigma)$, we choose the following gauge (See also [48])

$$\sqrt{2\dot{v}\dot{r} - \left(\frac{r}{L}\right)^{z+1} f(r)\dot{v}^2} = \left(\frac{r}{L}\right)^{\frac{z-1}{2}} \frac{r^{d_e - \theta_e}}{r_F^{-\theta_e(d+1)} L^d} a(r). \quad (3.5)$$

Now, one can compare the problem with that of the motion of a classical non-relativistic particle with action \mathcal{C}_{gen} [48]. In this manner, extremizing \mathcal{C}_{gen} gives the corresponding equations of motion for the particle. Having said this, since the metric (2.4) is stationary, the momentum P_v conjugate to the infalling time v is conserved¹⁰

$$P_v(\tau) = \dot{r} - \left(\frac{r}{L}\right)^{z+1} f(r)\dot{v} = \text{const.} \quad (3.6)$$

¹⁰It should be emphasized that P_v is a function of the boundary time τ and for a given value of τ it is a constant which is fixed by eq. (3.11).

Next, by solving eqs. (3.5) and (3.6), one has

$$\dot{r} = \pm \sqrt{P_v^2 + \frac{r^{2(d+z-\theta_e(d+1))}}{L^{2(d+z)}} r_F^{2\theta_e(d+1)} a(r)^2 f(r)}, \quad (3.7)$$

$$\dot{v} = \left(\frac{L}{r}\right)^{z+1} \frac{1}{f(r)} \left(-P_v \pm \sqrt{P_v^2 + \frac{r^{2(d+z-\theta_e(d+1))}}{L^{2(d+z)}} r_F^{2\theta_e(d+1)} a^2(r) f(r)} \right), \quad (3.8)$$

which extremize \mathcal{C}_{gen} . In this case, the position of the particle is given by the coordinate r . On the other hand, the effective potential $\hat{U}(r)$ is defined by

$$\dot{r}^2 + \hat{U}(r) = P_v^2. \quad (3.9)$$

Then from eq. (3.7) and (3.9), one can easily find the effective potential $\hat{U}(r)$ as follows

$$\hat{U}(r) = -\frac{r^{2(d+z-\theta_e(d+1))}}{L^{2(d+z)}} r_F^{2\theta_e(d+1)} a^2(r) f(r). \quad (3.10)$$

From the above expression and eqs. (3.4) and (3.16), it is obvious that $\hat{U}(r)$ becomes zero at $r = r_h$. Moreover, for $r < r_h$, one has $f(r) < 0$, and hence $\hat{U}(r)$ is positive in the range $0 < r < r_h$.¹¹ On the other hand, it is straightforward to show that for every value of the boundary time τ , the conserved momentum P_v is fixed by the following constraint

$$\tau = 2t_R = -2 \int_{r_{\min}}^{\infty} dr \frac{P_v}{\left(\frac{r}{L}\right)^{z+1} f(r) \sqrt{P_v^2 - \hat{U}(r)}}, \quad (3.11)$$

where r_{\min} is the minimal radius on the timelike surface $t = 0$ (See Figure 1) at which one has [21, 48]

$$\dot{r}|_{r=r_{\min}} = 0. \quad (3.12)$$

In other words, r_{\min} is the turning point of the particle moving in the potential $\hat{U}(r)$. On the other hand, from Figure 1, it is clear that r_{\min} is inside the horizon and at late times, one has $r_{\min} \rightarrow r_f$ [21, 48]. From eqs. (3.7), (3.10) and (3.12), one arrives at

$$\begin{aligned} P_v^2 &= -\frac{r_{\min}^{2(d+z-\theta_e(d+1))}}{L^{2(d+z)}} r_F^{2\theta_e(d+1)} a^2(r_{\min}) f(r_{\min}) \\ &= \hat{U}(r_{\min}). \end{aligned} \quad (3.13)$$

On the other hand, at the maximum $r = r_f$ of $\hat{U}(r)$, one has [21, 48]

$$\hat{U}(r_f) = P_\infty^2, \quad \hat{U}'(r_f) = 0, \quad \hat{U}''(r_f) \leq 0, \quad (3.14)$$

¹¹It should be pointed out that for the case $\lambda = 0$, one has $a(r) = 1$ and $\hat{U}(0) = 0$. However, for the case $\lambda \neq 0$, $a(r)$ is divergent at $r = 0$. Therefore, $\hat{U}(r)$ is also divergent at $r = 0$.

where $P_\infty = \lim_{\tau \rightarrow \infty} P_v(\tau)$. Notice that the first equation is a result of the fact that r_f also satisfies eq. (3.12) and hence eq. (3.13) (See also ref. [21]). For later convenience, we change the radial coordinate as follows

$$w = \left(\frac{r}{r_h} \right)^{d_e+z}. \quad (3.15)$$

For the metric (3.1), the square of the Weyl tensor is simply given by

$$C^2 = \frac{(d-1)}{(d+1)L^4} \left(\frac{r_h}{r_F} \right)^{4\theta_e} w^{\frac{4\theta_e}{d_e+z}-2} (d_e(d_e-z+2) - 2z(z-1)w)^2. \quad (3.16)$$

Then the effective potential (3.10) can be written as follows

$$\begin{aligned} \hat{U}(w) = & -\frac{r_h^{2(d_e+z-\theta_e)}}{L^{2(d+z)}} r_F^{2\theta_e(d+1)} w^{2(1-\frac{\theta_e}{d_e+z})} \left(1 - \frac{1}{w} \right) \\ & \times \left(1 + \lambda \frac{(d-1)}{(d+1)} \left(\frac{r_h}{r_F} \right)^{4\theta_e} w^{\frac{4\theta_e}{d_e+z}-2} (d_e(d_e-z+2) - 2z(z-1)w)^2 \right)^2. \end{aligned} \quad (3.17)$$

Since there is a factor of $f(r)$ in the effective potential, it becomes zero at the horizon where $w = 1$. Moreover, it is also zero on the singularity at $w = 0$.

3.1 Growth Rate

In this section, we calculate the growth rate of \mathcal{C}_{gen} . To this end, we proceed in the same way as ref. [21]. By changing the integral variable in eq. (3.3) from σ to r and applying eqs. (3.5) and (3.7)¹², one has

$$\begin{aligned} \mathcal{C}_{\text{gen}} = & 2 \frac{V_d}{G_N L} \int_{r_{\min}}^{r_{\max}} \frac{dr}{\dot{r}} \frac{r^{d_e-\theta_e}}{r_F^{-\theta_e(d+1)} L^d} \sqrt{-\left(\frac{r}{L}\right)^{2z} f(r) \dot{v}^2 + 2 \left(\frac{r}{L}\right)^{z-1} \dot{v} \dot{r} a(r)} \\ = & \frac{2V_d}{G_N L} \int_{r_{\min}}^{r_{\max}} \frac{dr}{\dot{r}} \frac{r^{2(d_e-\theta_e)}}{r_F^{-2\theta_e(d+1)} L^{2d}} \left(\frac{r}{L}\right)^{(z-1)} a(r)^2 \\ = & \frac{2V_d}{G_N L} \int_{r_{\min}}^{r_{\max}} \frac{dr}{\sqrt{P_v^2 + \frac{r^{2(d+z-\theta_e(d+1))}}{L^{2(d+z)}} r_F^{2\theta_e(d+1)} a(r)^2 f(r)} \frac{r^{2(d_e-\theta_e)}}{r_F^{-2\theta_e(d+1)} L^{2d}} \left(\frac{r}{L}\right)^{(z-1)} a(r)^2. \end{aligned} \quad (3.18)$$

On the other hand, by integrating $dv = dt + dr^*$ and applying eqs. (3.7) and (3.8), one has

$$\begin{aligned} t_R + r_\infty^* - r^*(r_{\min}) = & \int_{v_{\min}}^{v_\infty} dv = \int_{r_{\min}}^\infty dr \frac{\dot{v}}{\dot{r}} \\ = & \int_{r_{\min}}^{r_{\max}} \frac{dr}{f(r)} \left(\frac{L}{r}\right)^{z+1} \left[1 - \frac{P_v}{\sqrt{P_v^2 + \frac{r^{2(d+z-\theta_e(d+1))}}{L^{2(d+z)}} r_F^{2\theta_e(d+1)} a(r)^2 f(r)}} \right], \end{aligned}$$

¹²We choose the positive sign in eq. (3.7).

(3.19)

where $r_\infty^* = r^*(\infty)$. Next, by multiplying eq. (3.19)¹³ by P_v and adding it to eq. (3.18), one can rewrite the latter as follows

$$\mathcal{C}_{\text{gen}} = \frac{2V_d}{G_N L} \left\{ \int_{r_{\min}}^{r_{\max}} \frac{dr}{f(r)} \left(\frac{L}{r} \right)^{z+1} \left[\sqrt{P_v^2 + \frac{r^{2(d+z-\theta_e(d+1))}}{L^{2(d+z)}} r_F^{2\theta_e(d+1)} a(r)^2 f(r)} - P_v \right] + P_v (t_R + r_\infty^* - r^*(r_{\min})) \right\}. \quad (3.20)$$

Then, by taking the derivative of the above expression with respect to the time t_R , one obtains

$$\begin{aligned} \frac{d\mathcal{C}_{\text{gen}}}{dt_R} &= \frac{2V_d}{G_N L} \left\{ \frac{dP_v}{dt_R} \int_{r_{\min}}^{r_{\max}} dr \left(\frac{L}{r} \right)^{z+1} \frac{1}{f(r)} \left[\frac{P_v}{\sqrt{P_v^2 + \frac{r^{2(d+z-\theta_e(d+1))}}{L^{2(d+z)}} r_F^{2\theta_e(d+1)} a(r)^2 f(r)}} - 1 \right] \right. \\ &\quad \left. + \frac{dP_v}{dt_R} (t_R + r_\infty^* - r^*(r_{\min})) + P_v \right\} \\ &= P_v, \end{aligned} \quad (3.21)$$

where in the last line we applied eq. (3.19). Since $\tau = 2t_R$, one can rewrite the above equation as follows

$$\frac{d\mathcal{C}_{\text{gen}}}{d\tau} = \frac{V_d}{G_N L} P_v(\tau) = \frac{V_d}{G_N L} \sqrt{\hat{U}(r_{\min})}, \quad (3.22)$$

where we used eq. (3.13). At late times, $r_{\min} \rightarrow r_f$, and hence one has

$$\lim_{\tau \rightarrow \infty} \frac{d\mathcal{C}_{\text{gen}}}{d\tau} = \frac{V_d}{G_N L} P_\infty = \frac{V_d}{G_N L} \sqrt{\hat{U}(r_f)}. \quad (3.23)$$

Therefore, the growth rate of \mathcal{C}_{gen} at late times, is *linear* and determined by the value of the effective potential at $r = r_f$. Notice that r_f is a maximum of $\hat{U}(r)$ and is located inside the horizon. Therefore, the maximum of $\hat{U}(r)$ inside the horizon determines the growth rate of generalized volume-complexity at late times. In Section 3.3, we investigate such maxima.

Now, we want to prove that the generalized volume-complexity approaches its late time value in eq. (3.23) from below. To do so, we expand $\hat{U}(r_{\min})$ in eq. (3.22) around $r = r_f$ as follows

$$\frac{d\mathcal{C}_{\text{gen}}}{d\tau} = \frac{V_d}{G_N L} \left[\sqrt{\hat{U}(r_f)} + \frac{\hat{U}''(r_f)(r - r_f)^2}{4\sqrt{\hat{U}(r_f)}} + \mathcal{O}((r - r_f)^3) \right], \quad (3.24)$$

where we used the fact that $\hat{U}'(r_f) = 0$. Since r_f is a maximum of $\hat{U}(r)$, the second term in eq. (3.24) is negative and hence $\frac{d\mathcal{C}_{\text{gen}}}{d\tau}$ approaches its late time value from below. This behavior can be easily seen in Figures 2, 3, 4, 11, 12, 13 and 14.

¹³We change the upper limit of the integral in eq. (3.19) from ∞ to r_{\max} .

3.2 $\lambda = 0$: Volume-Complexity

As mentioned before, for the case $\lambda = 0$, one has $a(r) = 1$ and hence \mathcal{C}_{gen} reduces to the volume-complexity \mathcal{C}_V . Moreover, it is straightforward to check that the local maximum of $\hat{U}(r)$ is given by

$$r_f = r_h w_f^{\frac{1}{(d_e+z)}}, \quad (3.25)$$

where

$$w_f = \frac{d_e + z - 2\theta_e}{2d_e + 2z - 2\theta_e}. \quad (3.26)$$

Since $d_e > 0$ and $z \geq 1$, one has $d_e + z > 0$. Therefore, $w_f < 1$ and this maximum is located inside the horizon. Next, by plugging eq. (3.26) into eq. (3.23), one obtains the late time growth rate of \mathcal{C}_V as follows

$$\lim_{\tau \rightarrow \infty} \frac{d\mathcal{C}_V}{d\tau} = \frac{V_d}{2G_N} \frac{r_F^{\theta_e(d+1)} r_h^{d_e+z-\theta_e}}{L^{d+z+1}} \Upsilon, \quad (3.27)$$

where

$$\Upsilon = \frac{\sqrt{(d_e+z)((d+z)-(d+2)\theta_e)}}{((d+z)-(d+1)\theta_e)} \times \left(\frac{(d+z)-(d+2)\theta_e}{2(d+z)-2(d+1)\theta_e} \right)^{-\frac{\theta_e}{(d_e+z)}}. \quad (3.28)$$

Moreover, one can rewrite eq. (3.27) as follows

$$\begin{aligned} \lim_{\tau \rightarrow \infty} \frac{d\mathcal{C}_V}{d\tau} &= \frac{8\pi M^{1-\frac{\theta_e}{d_e+z}}}{d_e} r_F^{\theta_e(1+\frac{\theta_e}{d_e+z})} \left(\frac{16\pi G_N L^{d+z+1}}{V_d d_e} \right)^{-\frac{\theta_e}{d_e+z}} \Upsilon \\ &= \frac{8\pi M}{d_e} r_F^{\theta_e} \left(\frac{4\pi L^{z+1}}{d_e+z} \right)^{-\frac{\theta_e}{z}} \Upsilon T^{-\frac{\theta_e}{z}} \\ &= MT^{-\frac{\theta_e}{z}}. \end{aligned} \quad (3.29)$$

It should be pointed out that for another kind of HV black branes it was shown in ref. [23] that $\lim_{\tau \rightarrow \infty} \frac{d\mathcal{C}_V}{d\tau} \propto MT^{-\frac{\theta_e}{z}}$. On the other hand, for $\theta = 0$ and $z = 1$, the black brane solution becomes a planar AdS-Schwarzschild black hole whose mass is given by ¹⁴

$$\tilde{M} = \frac{d V_d r_h^{d+1}}{16\pi G_N L^{d+2}}. \quad (3.30)$$

In this case, $\Upsilon = 1$ and hence the late time growth rate of \mathcal{C}_V in eq. (3.29) reduces to

$$\lim_{\tau \rightarrow \infty} \frac{d\mathcal{C}_V}{d\tau} = \frac{V_d r_h^{d+1}}{2G_N L^{d+2}} = \frac{8\pi \tilde{M}}{d}, \quad (3.31)$$

which is the same as that for a planar AdS-black hole in ref. [21].

¹⁴As mentioned in footnote 9, one has $\Omega_d = \frac{V_d}{L^d}$. Therefore, the mass of a planar AdS-Schwarzschild black hole is also written as $M = \frac{d \Omega_d r_h^{d+1}}{16\pi G_N L^2}$.

3.2.1 General Time Dependence

In this section, we want to numerically calculate the time dependence of the volume-complexity for an arbitrary time. To this end, we first define (See also [21])

$$s = \frac{r}{r_h}, \quad s_{\min} = \frac{r_{\min}}{r_h}, \quad (3.32)$$

and the normalized growth rate

$$\alpha = \frac{\frac{dC_V}{d\tau}}{\lim_{\tau \rightarrow \infty} \frac{dC_V}{d\tau}}, \quad (3.33)$$

where the late time growth rate is given in eq. (3.29). Then by applying eqs. (3.10) and (3.27), one can rewrite eq. (3.22) as follows

$$\alpha = \frac{2}{\Upsilon} s_{\min}^{\frac{d_e+z}{2}-2\theta_e} \sqrt{1 - s_{\min}^{d_e+z}}. \quad (3.34)$$

On the other hand, by applying eqs. (2.12) and (3.13), one can recast eq. (3.19) to the following form ¹⁵

$$\tau = \frac{(d_e + z)\beta\alpha L}{4\pi} \int_{s_{\min}}^{\infty} ds \frac{s^{d_e-1}}{(1 - s^{d_e+z}) \sqrt{s_{\min}^{d_e+z-2\theta_e} (1 - s_{\min}^{d_e+z}) - s^{d_e+z-2\theta_e} (1 - s^{d_e+z})}}, \quad (3.35)$$

where β is the inverse temperature. In Figures 2, 3 and 4, we plotted the normalized growth rate α as a function of $\frac{\tau}{\beta}$ for different values of d , θ and z . It is observed that, for all values of d , θ and z , C_V approaches its late time value given in eq. (3.29) from *below* which verifies the discussion below eq. (3.24). Moreover, from Figure 2, it is observed that α is an increasing function of d . In Figure 3, α is a decreasing function of z . On the other hand, in Figure 4, it is observed that for $\{d = 1, z = 1\}$, α is an increasing function of θ . However, for $\{d = 2, z = 5\}$, $\{d = 3, z = \frac{9}{2}\}$ and $\{d = 4, z = 6\}$ it is a decreasing function of θ . It should be pointed out that for $\theta = 0$ and $z = 1$, the behavior of the growth rate is again the same as that in ref. [21].

3.3 Maxima of the Effective Potential For $\lambda \neq 0$

In this section, we investigate the local maxima w_f of the effective potential $\hat{U}(w)$ ¹⁶ which are located inside the horizon, i.e.

$$\hat{U}''(w_f) < 0, \quad 0 < w_f < 1. \quad (3.36)$$

¹⁵Notice that $0 < s_{\min} < 1$ and $s > s_{\min}$. Moreover, depending on the values of d , θ and z , for some values of s_{\min} , τ becomes imaginary and one has to discard them. Furthermore, the integrand is singular at $s = 1$. To avoid the singularity in the numerical calculations, we changed the limit of the integral in eqs. (3.35) and (3.57) as follows $\int_{s_{\min}}^{\infty} ds F(s) = \int_{s_{\min}}^{1-\epsilon} ds F(s) + \int_{1+\epsilon}^{\infty} ds F(s)$, where $\epsilon = 2 \times 10^{-8}$.

¹⁶For convenience, we work in the w coordinate instead of r in this section. The two coordinates are related to each other by eq. (3.15).

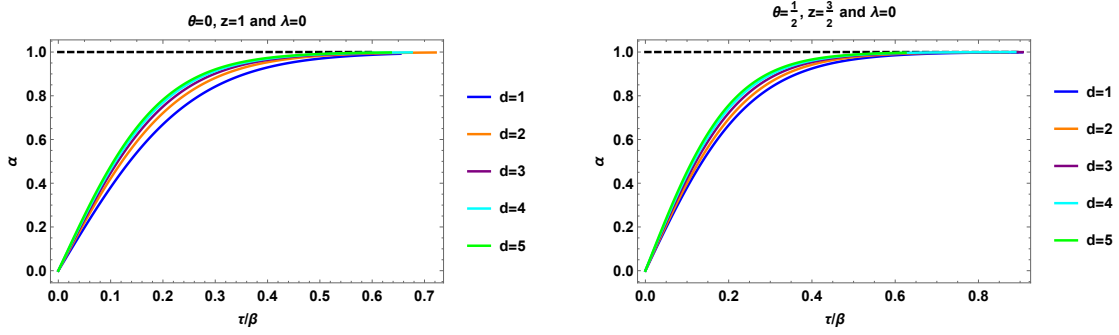


Figure 2. The normalized growth rate $\alpha = \frac{\frac{dC_V}{d\tau}}{\lim_{\tau \rightarrow \infty} \frac{dC_V}{d\tau}}$ as a function of τ/β for $\lambda = 0$ and different values of d , θ and z : *Left*) $\theta = 0$ and $z = 1$. This figure is the same as Figure 7 in ref. [48], since for these values of θ and z , the black brane becomes a planar AdS-Schwarzschild black hole. *Right*) $\theta = \frac{1}{2}$ and $z = \frac{3}{2}$. We set $L = r_h = r_F = 1$.

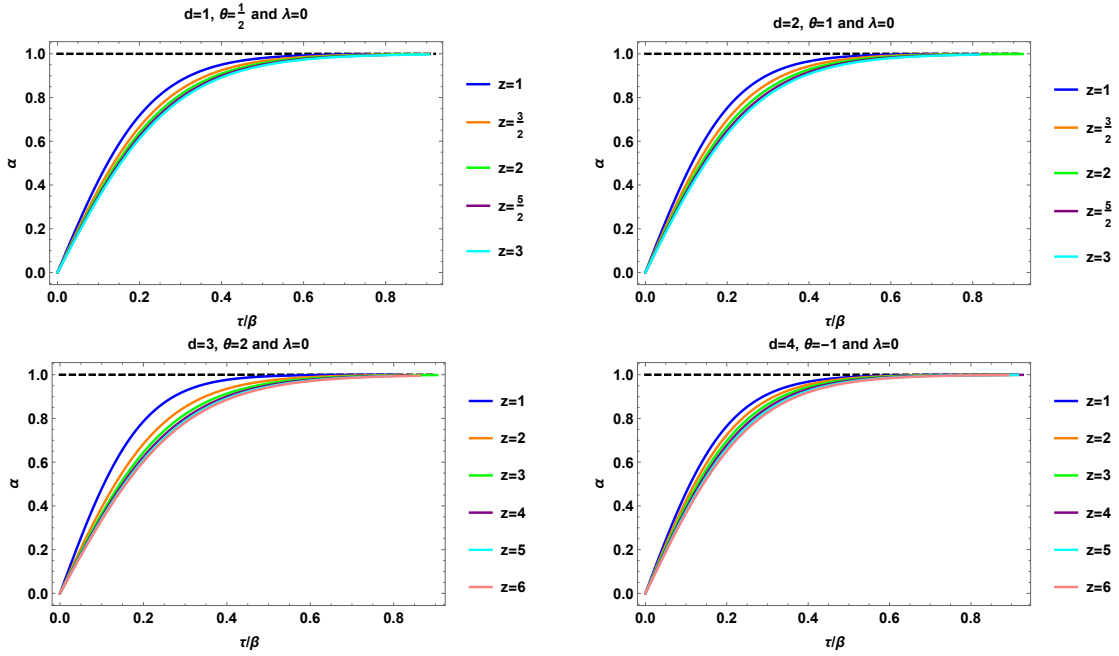


Figure 3. The normalized growth rate α as a function of τ/β for $\lambda = 0$ and different values of d , θ and z : *Top Left*) $d = 1$ and $\theta = \frac{1}{2}$, *Top Right*) $d = 2$ and $\theta = 1$, *Down Left*) $d = 3$ and $\theta = 2$, *Down Right*) $d = 4$ and $\theta = -1$. We set $L = r_h = r_F = 1$.

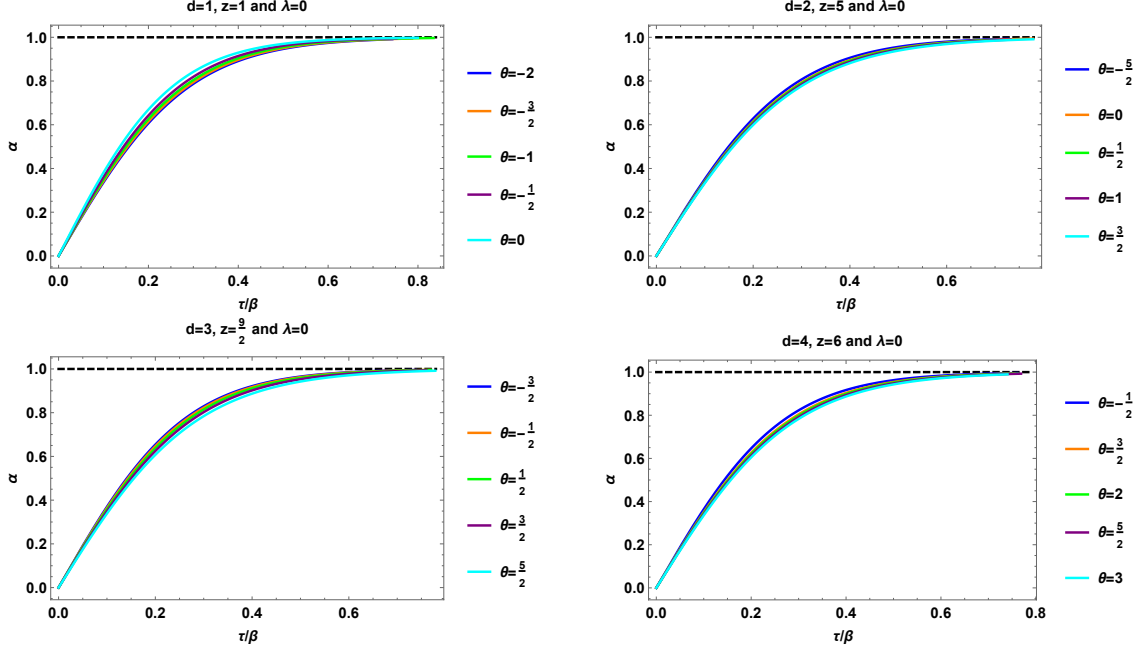


Figure 4. The normalized growth rate α as a function of τ/β for $\lambda = 0$ and different values of d , θ and z : *Top Left*) $d = 1$ and $z = 1$, *Top Right*) $d = 2$ and $z = 5$, *Down Left*) $d = 3$ and $z = \frac{9}{2}$, *Down Right*) $d = 4$ and $z = 6$. We set $L = r_h = r_F = 1$.

As mentioned below eq. (3.23), these maxima determine the growth rate of C_{gen} at late times. For the case $\lambda = 0$, we found the local maximum of $\hat{U}(r)$ in eq. (3.25). In the following, we consider the case $\lambda \neq 0$. In this case, by taking the derivative of $\hat{U}(w)$ with respect to w , one has

$$\frac{d\hat{U}(w)}{dw} = \frac{A(\lambda, w)B(\lambda, w)}{w^{1+\frac{2\theta_e}{d_e+z}}}, \quad (3.37)$$

where

$$A(\lambda, w) = d + 1 + (d - 1) \left(\frac{r_h}{r_F} \right)^{4\theta_e} w^{-2+\frac{4\theta_e}{d_e+z}} (2wz(z-1) - d_e(d_e - z + 2))^2 \lambda, \quad (3.38)$$

$$B(\lambda, w) = B_0(w) + \lambda B_1(w), \quad (3.39)$$

and the functions $B_{0,1}(w)$ are defined as follows

$$B_0(w) = -w(d+1)(d(2w-1)(d+z) + (d+2-2(d+1)w)\theta),$$

$$B_1(w) = \left(\frac{r_h}{r_F} \right)^{4\theta_e} \frac{(d-1)}{w^{1-\frac{4\theta_e}{d_e+z}}} (d^2 - 2wz(z-1) + \theta(\theta+z-2) - d(z+2(\theta-1))) \\ \times \left[4(w-1) \left(\theta((d+4w)z^2 - d(4+3d(d+2))) - 4zw \right) \right]$$

$$\begin{aligned}
& +d^2(d-z+2)(d+z) + (4+3d(d+2)-2z)\theta^2 - (d+2)\theta^3 \\
& + \left(d(d_e+z)(1-2w) + 2(w-1)\theta \right) \\
& \times \left(d^2 - 2wz(z-1) + \theta(z+\theta-2) - d(z+2(\theta-1)) \right) \Big].
\end{aligned} \tag{3.40}$$

By setting $A(\lambda, w) = 0$ or $B(\lambda, w) = 0$, one can find λ in terms of w as follows

$$\lambda = - \left(\frac{r_F}{r_h} \right)^{4\theta_e} \frac{(d+1)w^{2-\frac{4\theta_e}{d_e+z}}}{(d-1)(2z(z-1)w - d_e(d_e-z+2))^2}, \tag{3.41}$$

$$\lambda = - \frac{B_0(w)}{B_1(w)}, \tag{3.42}$$

respectively. Next, from the above equations, one can find the extrema w of $\hat{U}(w)$. However, it is not possible to solve eqs. (3.41) and (3.42) analytically for arbitrary values of d , θ and z . Therefore, in the following we consider some specific values of these parameters for which there are analytic solutions.

3.3.1 $\theta = 0$

In this case, the background becomes a Lifshitz black brane. Moreover, it is straightforward to show that eq. (3.41) has the following solutions when $d \neq 1$

$$w_{fA1} = \frac{d \left(2z(d-1)(d-z+2)(z-1)\lambda + \sqrt{\lambda(1-d^2)}|d-z+2| \right)}{d+1+4(d-1)(z-1)^2z^2\lambda}, \tag{3.43}$$

$$w_{fA2} = \frac{d \left(2z(d-1)(d-z+2)(z-1)\lambda - \sqrt{\lambda(1-d^2)}|d-z+2| \right)}{d+1+4(d-1)(z-1)^2z^2\lambda}. \tag{3.44}$$

It is clear that to have a real value for $w_{fA1,2}$, one needs $\lambda < 0$. Moreover, asking for $w_{fA1,2}$ to be a local maximum, i.e. $\hat{U}''(w_{fA1,2}) < 0$, imposes a constraint on the value of λ . These values are reported in Tables 1 and 2, respectively. It is straightforward to verify that for these values of λ , $w_{fA1,2}$ are always located outside the horizon. Therefore, they have no contributions to the late time growth rate of \mathcal{C}_{gen} , and we are not interested to them here. In Figures 5 and 6, we plotted $\hat{U}(w)$ for $\theta = 0$ and different values of d and z . It is observed that $w_{fA1,2}$ are maxima of $\hat{U}(w)$ and located *outside* the horizon, i.e. $w_{fA1,2} > 1$. On the other hand, for $d = 1$, from eq. (3.38), one has $A(\lambda, w) = d + 1$. Therefore, equation $A(\lambda, w) = 0$, has no solutions.

Next, we find the maxima given by eq. (3.42). By setting $\theta = 0$, it simplifies to

$$\lambda = \frac{(d+1)w^2(2w-1)}{(d-1)(d^2-d(z-2)-2wz(z-1))(d^2(2w-3)-d(2w-3)(z-2)+2z(z-1)w(2w-1))},$$

| | $d = 2$ | $d = 3$ | $d = 4$ | $d = 5$ |
|---------|---|---|----------------------------|----------------------------|
| $z = 1$ | $\lambda < -\frac{1}{12}$ | $\lambda < -\frac{1}{72}$ | $\lambda < -\frac{1}{240}$ | $\lambda < -\frac{1}{600}$ |
| $z = 2$ | $\hat{U}''(w_{fA}) > 0$ | $\lambda < -\frac{2}{25}$ | $\lambda < -\frac{5}{432}$ | $\lambda < -\frac{1}{294}$ |
| $z = 3$ | $\hat{U}''(w_{fA}) > 0$ | $\hat{U}''(w_{fA}) > 0$ | $\hat{U}''(w_{fA}) > 0$ | $\lambda < -\frac{3}{128}$ |
| $z = 4$ | $w_{fA} = 0$ | $\hat{U}''(w_{fA}) > 0$ | $\hat{U}''(w_{fA}) > 0$ | $\hat{U}''(w_{fA}) > 0$ |
| $z = 5$ | $-\frac{3}{1600} < \lambda < -\frac{1}{588}$ | $w_{fA} = 0$ | $\hat{U}''(w_{fA}) > 0$ | $\hat{U}''(w_{fA}) > 0$ |
| $z = 6$ | $-\frac{1}{1200} < \lambda < -\frac{3}{4096}$ | $-\frac{1}{1800} < \lambda < -\frac{2}{3969}$ | $w_{fA} = 0$ | $\hat{U}''(w_{fA}) > 0$ |

Table 1. The appropriate ranges of the coupling constant λ for which w_{fA1} is a maximum outside the horizon. For some values of d and z , one has $\hat{U}''(w_{fA1}) > 0$. In these cases, w_{fA1} is a minimum. Moreover, for some cases, one has $w_{fA1} = 0$, which should be discarded.

| | $d = 2$ | $d = 3$ | $d = 4$ | $d = 5$ |
|---------|--|---|--|---|
| $z = 1$ | There is no λ | There is no λ | There is no λ | There is no λ |
| $z = 2$ | $\lambda < -\frac{3}{16}$ | $\lambda < -\frac{1}{8}$ | $\lambda < -\frac{5}{48}$ | $\lambda < -\frac{3}{32}$ |
| $z = 3$ | $-\frac{3}{100} < \lambda < -\frac{1}{48}$ | $-\frac{1}{18} < \lambda < -\frac{1}{72}$ | $\lambda < -\frac{5}{432}$ | $\lambda < -\frac{1}{96}$ |
| $z = 4$ | There is no λ | $-\frac{2}{441} < \lambda < -\frac{1}{288}$ | $-\frac{5}{768} < \lambda < -\frac{5}{1728}$ | $-\frac{1}{54} < \lambda < -\frac{1}{384}$ |
| $z = 5$ | There is no λ | There is no λ | $-\frac{5}{3888} < \lambda < -\frac{1}{960}$ | $-\frac{1}{600} < \lambda < -\frac{3}{3200}$ |
| $z = 6$ | There is no λ | There is no λ | There is no λ | $-\frac{3}{6050} < \lambda < -\frac{1}{2400}$ |

Table 2. The appropriate ranges of the coupling constant λ for which w_{fA2} is a maximum outside the horizon. For some cases, there is no λ .

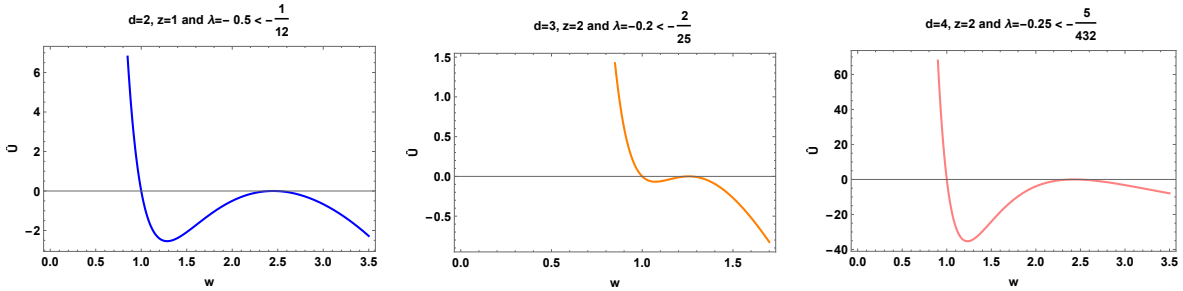


Figure 5. The effective potential $\hat{U}(w)$ as a function of w for $\theta = 0$ and different values of d , z and λ . For the values of λ given in Table 1, there is a maximum w_{fA1} outside the horizon, i.e. $w_{fA1} > 1$. We set $L = r_h = r_F = 1$.

(3.45)

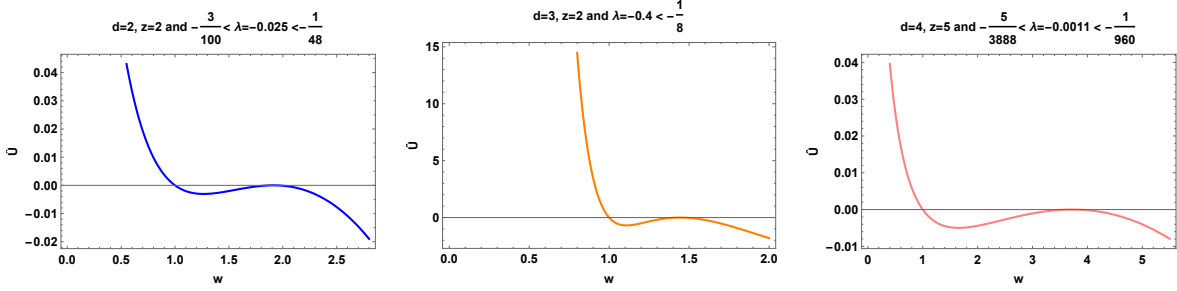


Figure 6. The effective potential $\hat{U}(w)$ as a function of w for $\theta = 0$ and different values of d , z and λ . For the values of λ given in Table 2, there is a maximum w_{fA2} outside the horizon.

| | $d = 2$ | $d = 3$ | $d = 4$ | $d = 5$ |
|---------|---|---|---|---|
| $z = 1$ | $\lambda > \frac{1}{12}\lambda_{crt,2}$ | $\lambda > \frac{1}{72}\lambda_{crt,2}$ | $\lambda > \frac{1}{240}\lambda_{crt,2}$ | $\lambda > \frac{1}{600}\lambda_{crt,2}$ |
| $z = 2$ | There is no λ | $\lambda > \frac{655+23\sqrt{805}}{5300}$ | $\lambda > \frac{2777+103\sqrt{721}}{100224}$ | $\lambda > \frac{27947+323\sqrt{742s9}}{2655408}$ |
| $z = 3$ | There is no λ | There is no λ | There is no λ | $\lambda > \frac{11391+381\sqrt{889}}{418816}$ |
| $z = 4$ | There is no λ | There is no λ | There is no λ | There is no λ |
| $z = 5$ | There is no λ | There is no λ | There is no λ | There is no λ |
| $z = 6$ | There is no λ | There is no λ | There is no λ | There is no λ |

Table 3. The appropriate ranges of the coupling constant λ for which w_{fB} is a maximum outside the horizon. Here, $\lambda_{crt,2}$ is defined by eq. (3.52).

from which one can find another extremum w_{fB} .¹⁷ Since the corresponding expression is very complicated, we do not write it here. However, for $\lambda \ll 1$, one can expand it in powers of λ as follows

$$\begin{aligned}
w_{fB} = & \frac{1}{2} - \frac{4d(d-1)(d-z+2)(d(d+2)+z(1-d-z))}{(d+1)}\lambda \\
& - \frac{16(d-1)^2}{(d+1)^2}d(d-z+2)(d(d+2)+z(1-d-z)) \times \left(5d^2(d+2)^2 - 2d(d+2)(5d-1)z \right. \\
& \left. + (-1+3d(d-2))z^2 + 2(d+1)z^3 - z^4 \right) \lambda^2 + \mathcal{O}(\lambda^3) + \dots .
\end{aligned} \tag{3.46}$$

It should be pointed out that w_{fB} can be a local maximum either *outside* or *inside* the horizon depending on the value of the coupling λ . The corresponding values of λ are shown in Tables 3 and 4, respectively. According to Table 3, it is easy to see that for $z = 4, 5, 6$, w_{fB} cannot be a maximum outside the horizon when $d = 2, 3, 4, 5$. On the other hand, from Table 4, for every values

¹⁷It should be emphasized that eq. (3.45) gives three extrema w_{fB1} , w_{fB2} and w_{fB3} . The extrema w_{fB2} and w_{fB3} generally have imaginary parts. However, for some values of λ , the ratio of their imaginary parts to their real parts can be as small as 10^{-15} or 10^{-16} . In the following, we discard $w_{fB2,3}$ and denote w_{fB1} by w_{fB} .

| | $d = 2$ | $d = 3$ | $d = 4$ | $d = 5$ |
|---------|---|---|--|---|
| $z = 1$ | $-\frac{1}{12} < \lambda < \frac{1}{12} \lambda_{crt,1}$ | $-\frac{1}{72} < \lambda < \frac{1}{72} \lambda_{crt,1}$ | $-\frac{1}{240} < \lambda < \frac{1}{240} \lambda_{crt,1}$ | $-\frac{1}{600} < \lambda < \frac{1}{600} \lambda_{crt,1}$ |
| $z = 2$ | $-\frac{3}{16} < \lambda < \frac{9}{2000}$ | $-\frac{2}{25} < \lambda < \frac{655-23\sqrt{805}}{5300}$ | $-\frac{5}{432} < \lambda < \frac{2777-103\sqrt{721}}{100224}$ | $-\frac{1}{294} < \lambda < \frac{27947-323\sqrt{7429}}{2655408}$ |
| $z = 3$ | $\lambda > -\frac{1}{48}$ | $\lambda > -\frac{1}{72}$ | $-\frac{5}{432} < \lambda < 0$ | $-\frac{1}{96} < \lambda < \frac{11391-381\sqrt{889}}{418816}$ |
| $z = 4$ | $\lambda > -\frac{1}{192}$ | $\lambda > -\frac{1}{288}$ | $-\frac{5}{1728} < \lambda < 0$ | $-\frac{1}{384} < \lambda < 0$ |
| $z = 5$ | $\lambda > -\frac{1}{588}$ | $\lambda > -\frac{1}{800}$ | $-\frac{1}{960} < \lambda < 0$ | $-\frac{3}{3200} < \lambda < 0$ |
| $z = 6$ | $-\frac{3}{4096} < \lambda < \frac{3(547+41\sqrt{697})}{2326528}$ | $\lambda > -\frac{2}{3969}$ | $w_{fB} = \frac{1}{2}$ and $\lambda > -\frac{1}{2160}$ | $-\frac{1}{2400} < \lambda < 0$ |

Table 4. The appropriate ranges of the coupling constant λ for which w_{fB} is a maximum inside the horizon. Here, $\lambda_{crt,1}$ is defined by eq. (3.52).

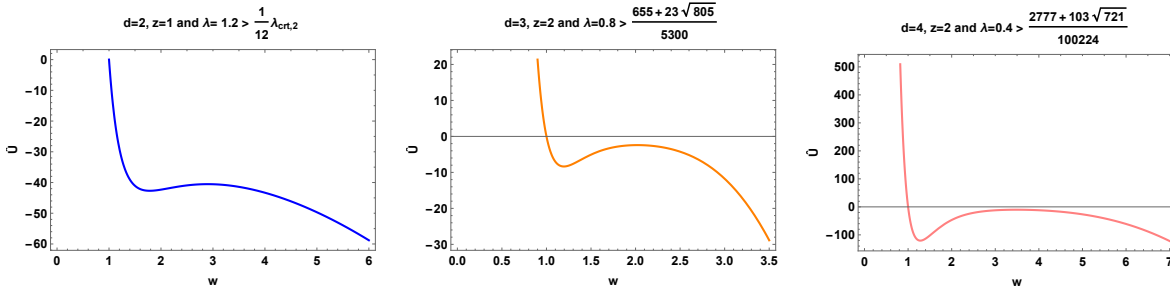


Figure 7. The effective potential $\hat{U}(w)$ as a function of w for $\theta = 0$ and different values of d , z and λ . For the values of λ given in Table 3 there is a maximum w_{fB} outside the horizon.

of d and z there is always a range of λ for which w_{fB} is a maximum inside the horizon. In Figures 7 and 8, we plotted $\hat{U}(w)$ as a function of w for the case $\theta = 0$ and different values of d and z to show its maxima. Figure 7 indicates that for the values of λ in Table 3, w_{fB} is a maximum outside the horizon. Moreover, Figure 8 shows that for the values of λ given in Table 4, w_{fB} is a maximum inside the horizon. Therefore, for the case $\theta = 0$, the only ranges of λ that we are interested in are given by Table 4. On the other hand, for the case $d = 1$, from eq. (3.39), one has

$$B(\lambda, w) = 4w(1 - 2w), \quad (3.47)$$

which is independent of λ . In this case, equation $B(\lambda, w) = 0$ gives two extrema $w = \{0, \frac{1}{2}\}$. The first one coincides with the singularity and should be discarded. The second one is a maximum inside the horizon. Therefore, for $d = 1$, $w_{fB} = \frac{1}{2}$ is always a maximum inside the horizon (See Figure 9) and in this case there is no constraint on the value of λ .

Eventually, by plugging eq. (3.46) into eq. (3.23), one obtains the late time growth rate as follows

$$\lim_{\tau \rightarrow \infty} \frac{d\mathcal{C}_{\text{gen}}}{d\tau} = \frac{8\pi M}{d} \left[1 + \frac{4(d-1)(d(d+2) + z(1-d-z))^2}{d+1} \lambda + 2 \left(\frac{4d(d-1)(d-z+2)(d(d+2) + z(1-d-z))}{d+1} \right)^2 \lambda^2 + \mathcal{O}(\lambda^3) + \dots \right], \quad (3.48)$$

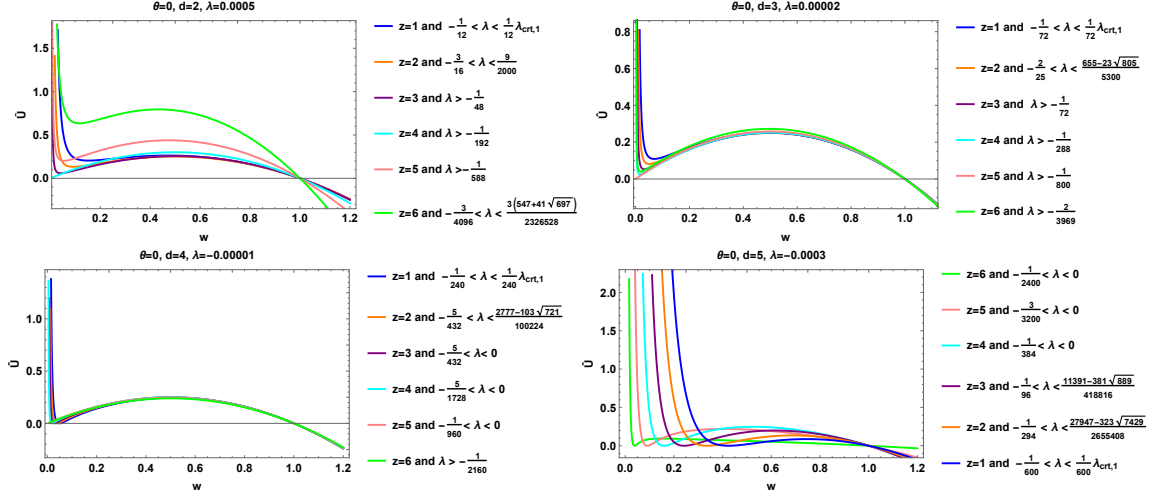


Figure 8. The effective potential $\hat{U}(w)$ as a function of w for $\theta = 0$ and different values of d and z . For all values of z , there is a maximum w_{fB} inside the horizon. The appropriate ranges of λ are given in Table 4.

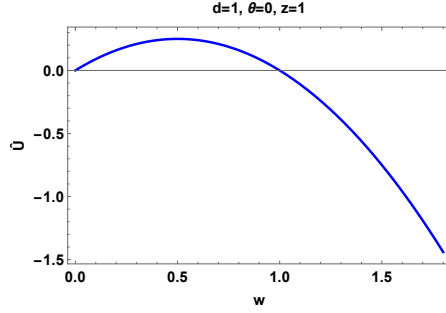


Figure 9. The effective potential $\hat{U}(w)$ as a function of w for $d = 1$, $\theta = 0$ and $z = 1$. In this case, $\hat{U}(w)$ is independent of λ , and there is a maximum inside the horizon at $w_{fB} = \frac{1}{2}$.

where for $\lambda = \theta = 0$, it is consistent with eq. (3.29). Moreover, for $d = 1$, one arrives at

$$\lim_{\tau \rightarrow \infty} \frac{d\mathcal{C}_{\text{gen}}}{d\tau} = 8\pi M, \quad (3.49)$$

which is independent of λ .

3.3.2 $\theta = 0$ and $z = 1$

For $\theta = 0$ and $z = 1$, the background becomes a planar AdS-Schwarzschild black hole. In this case, the exact expression for w_{fB} is easily obtained as follows

$$w_{fB} = \frac{1}{6} \left(1 + \frac{1 + 12\tilde{\lambda}}{\left(1 - 144\tilde{\lambda} + 6\sqrt{3}\sqrt{-\tilde{\lambda}(4\tilde{\lambda}(4\tilde{\lambda} - 47) + 3)} \right)} \right)^{\frac{1}{3}}$$

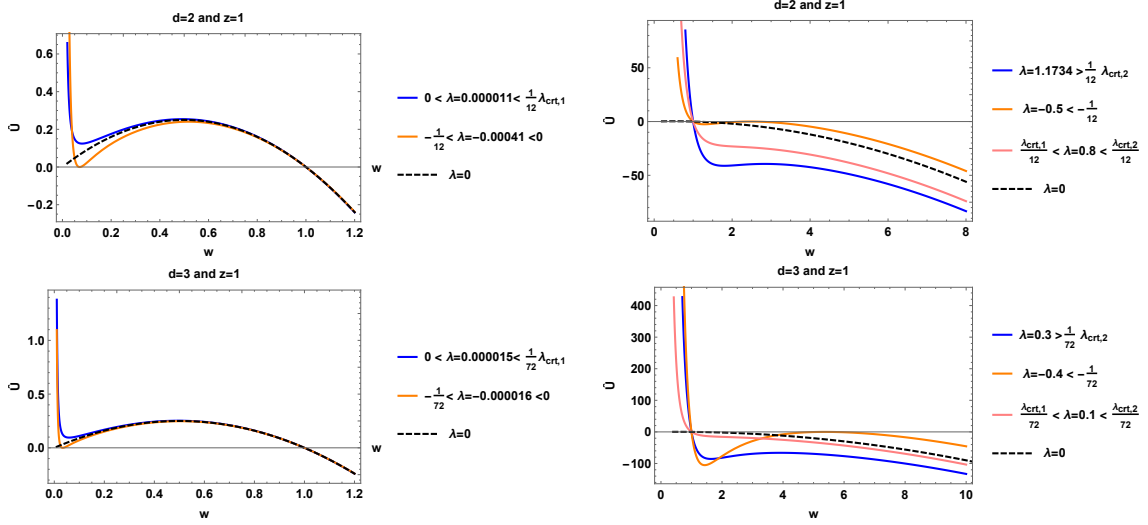


Figure 10. The effective potential $\hat{U}(w)$ as a function of $w = \left(\frac{r}{r_h}\right)^{d_e+z}$ for $\theta = 0$, $z = 1$ and different values of d and λ . *Left*) when $\lambda = 0$, $0 < \tilde{\lambda} < \lambda_{crit,1}$ and $-1 < \tilde{\lambda} < 0$, there is a local maximum w_{fB} inside the horizon (See Table 4). *Right*) when $\tilde{\lambda} > \lambda_{crit,2}$ and $\tilde{\lambda} < -1$ there are two maxima w_{fA1} and w_{fB} which are located outside the horizon (See Tables 1 and 3). For $\lambda_{crit,1} < \tilde{\lambda} < \lambda_{crit,2}$ there is no maximum. In the first row $d = 2$ and in the second row $d = 3$. Notice that for $d = 2, 3$ one has $\tilde{\lambda} = 12\lambda$ and $\tilde{\lambda} = 72\lambda$, respectively. We also plotted the case $\lambda = 0$, i.e. the volume-complexity, which is indicated by the dashed black curve. We set $L = r_h = r_F = 1$. Since for these values of θ and z , the HV black brane becomes a planar AdS-Schwarzschild black hole, these figures are the same as Figure 3 in ref. [48].

$$+ \left(1 - 144\tilde{\lambda} + 6\sqrt{3}\sqrt{-\tilde{\lambda}(4\tilde{\lambda}(4\tilde{\lambda} - 47) + 3)}\right)^{\frac{1}{3}}, \quad (3.50)$$

where the effective coupling constant $\tilde{\lambda}$ is defined as follows

$$\tilde{\lambda} = d^2(d^2 - 1)\lambda. \quad (3.51)$$

It should be pointed out that w_{fB} in eq. (3.50) is the same as the maximum reported in ref. [48] for a planar AdS-Schwarzschild black hole. Moreover, for $z = 1$, when $-1 < \tilde{\lambda} < \lambda_{crit,1}$ and $\tilde{\lambda} > \lambda_{crit,2}$, w_{fB} is a maximum located inside and outside the horizon, respectively (See Figure 10) where the critical values for λ are defined as follows (See also [48])

$$\lambda_{crit,1} = \frac{1}{8}(47 - 13\sqrt{13}), \quad \lambda_{crit,2} = \frac{1}{8}(47 + 13\sqrt{13}). \quad (3.52)$$

Furthermore, for $\lambda_{crit,1} < \tilde{\lambda} < \lambda_{crit,2}$, there is no real w_{fB} . In Figure 10, we restricted ourselves to the case $z = 1$. In the left panels of Figure 10, the maxima are located inside the horizon. However, in the right panels of Figure 10, either there is no maximum or it is located outside the horizon. Next,

by plugging eq. (3.50), into eq. (3.23), one has

$$\lim_{\tau \rightarrow \infty} \frac{d\mathcal{C}_{\text{gen}}}{d\tau} = \frac{16\pi M}{d} \sqrt{w_{fB} - w_{fB}^2} \left(1 + \frac{\tilde{\lambda}}{w_{fB}^2} \right). \quad (3.53)$$

Notice that for $\lambda = 0$, one has $w_{fB} = \frac{1}{2}$, and hence eq. (3.53) reduces to eq. (3.31). It should also be pointed out that for some values of d, θ, z and λ , the potential $\hat{U}(w)$ may have two maxima (See the left panel of Figures 18 and 19). In the left panel of Figure 18, there is a maximum inside the horizon and there is another one outside the horizon. On the other hand, in the left panel of Figure 19, both maxima are located outside the horizon.

3.3.3 $d = 2, \theta = 1$ and $z = 1$

In this case, equation $A(\lambda, w) = 0$ has a solution which is a maximum outside the horizon. On the other hand, equation $B(\lambda, w) = 0$ has the following solution

$$w_{fB} = \frac{3r_F^2 + 4r_h^2\lambda - \sqrt{9r_F^2 - 408r_F^2r_h^2\lambda + 16r_h^4\lambda^2}}{18r_F^2}. \quad (3.54)$$

It is easy to verify that for

$$0 < \lambda < \frac{3(17 - 12\sqrt{2})r_F^2}{4r_h^2}, \quad (3.55)$$

w_{fB} is a maximum inside the horizon. Next, it is straightforward to calculate the late time value of \mathcal{C}_{gen} from eqs. (3.23) and (3.54).

3.4 General Time Dependence for $\lambda \neq 0$ and Arbitrary Values of θ and z

In this section, we calculate the time dependence of the growth rate of \mathcal{C}_{gen} . For $\lambda \neq 0$, it is straightforward to rewrite eq. (3.22) as follows

$$\frac{d\mathcal{C}_{\text{gen}}}{d\tau} = \frac{V_d r_h^{d_e+z-\theta_e} r_F^{\theta_e(d+1)}}{G_N L^{d+z+1}} s_{\text{min}}^{\frac{d_e+z}{2}-\theta_e} \sqrt{1 - s_{\text{min}}^{d_e+z}} a(s_{\text{min}}). \quad (3.56)$$

Moreover,

$$\begin{aligned} \tau = & \frac{(d_e + z)\beta a(s_{\text{min}}) s_{\text{min}}^{\frac{d_e+z}{2}-\theta_e} \sqrt{1 - s_{\text{min}}^{d_e+z}}}{2\pi} \\ & \times \int_{s_{\text{min}}}^{\infty} ds \frac{s^{d_e-1}}{(1 - s^{d_e+z}) \sqrt{s_{\text{min}}^{d_e+z-2\theta_e} (1 - s_{\text{min}}^{d_e+z}) a(s_{\text{min}})^2 - s^{d_e+z-2\theta_e} (1 - s^{d_e+z}) a(s)^2}}, \end{aligned} \quad (3.57)$$

where

$$a(s) = 1 + \lambda \frac{(d-1)}{(d+1)} \left(\frac{r_h}{r_F} \right)^{4\theta_e} s^{4\theta_e-2(d_e+z)} (d_e(d_e - z + 2) - 2z(z-1)s^{d_e+z})^2. \quad (3.58)$$

In Figures 11, 12, 13 and 14, we numerically plotted the growth rate $\frac{d\mathcal{C}_{\text{gen}}}{d\tau}$ as a function of τ/β for different values of d, θ, z and λ . From these figures, it is clear that for all values of d, θ and z , the

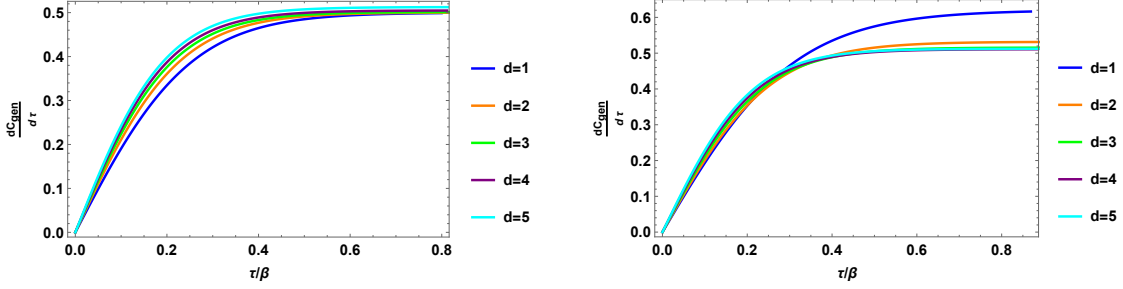


Figure 11. The growth rate $\frac{dC_{\text{gen}}}{d\tau}$ in eq. (3.22), as a function of τ/β for $\lambda \neq 0$ and different values of d , θ and z : *Left*) $\theta = 0$, $z = 1$, *Right*) $\theta = \frac{1}{2}$, $z = \frac{3}{2}$. We set $L = r_h = r_F = G_N = V_d = 1$ and $\lambda = 10^{-5}$.

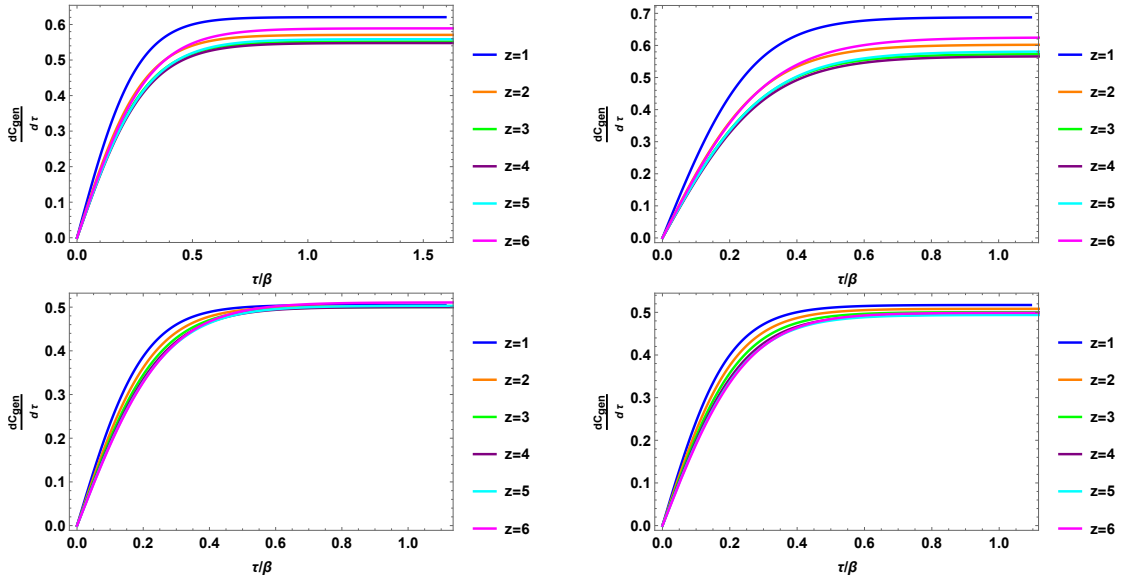


Figure 12. The growth rate $\frac{dC_{\text{gen}}}{d\tau}$ as a function of τ/β for $\lambda \neq 0$ and different values of d , θ and z : *Top Left*) $d = 2$, $\theta = 1$ and $\lambda = 10^{-4}$. *Top Right*) $d = 3$, $\theta = 2$ and $\lambda = 10^{-4}$. *Down Left*) $d = 4$ and $\theta = 0$ and $\lambda = 10^{-5}$. *Down Right*) $d = 5$ and $\theta = -1$ and $\lambda = 10^{-5}$. We set $L = r_h = r_F = G_N = V_d = 1$.

growth rate of generalized volume-complexity saturates at late times as it was argued below eq. (3.24) (See also ref. [48]). Moreover, it reaches its late time value from below as it was expected.

Furthermore, from Figures 11 and 12, it is observed that the growth rate is neither an increasing nor a decreasing function of d and z . Furthermore, from Figure 13, it is evident that $\frac{dC_{\text{gen}}}{d\tau}$ is an increasing function of θ which is in contrast to the case for $\lambda = 0$ (See Figure 4).

On the other hand, from eq. (3.58), it is clear that for a given value of d , θ and z , $a(s)$ is an increasing function of λ . Therefore, $\frac{dC_{\text{gen}}}{d\tau}$ is also an increasing function of λ .¹⁸ To verify this behavior, we also

¹⁸This behavior can also be seen from eqs. (3.17) and (3.22). It is clear that $\hat{U}(w)$ is an increasing function of λ .

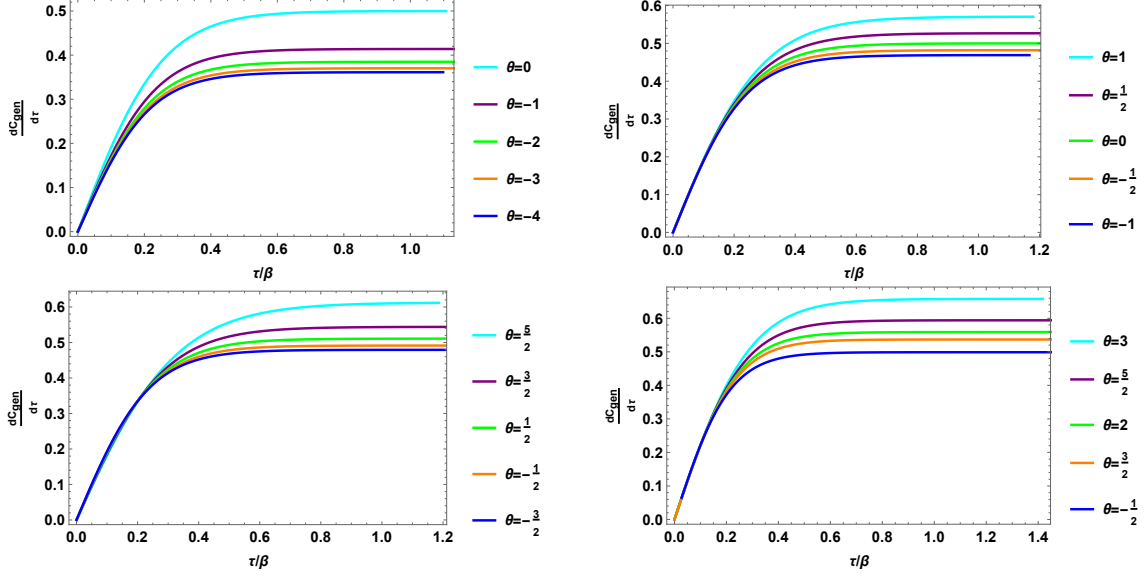


Figure 13. The growth rate $\frac{dC_{\text{gen}}}{dr}$ as a function of τ/β for $\lambda \neq 0$ and different values of d , θ and z : *Top Left*) $d = 1$, $z = 1$, *Top Right*) $d = 2$, $z = 2$, *Down Left*) $d = 3$ and $z = 3$, *Down Right*) $d = 4$ and $z = \frac{3}{2}$. We set $L = r_h = r_F = G_N = V_d = 1$ and $\lambda = 10^{-5}$.

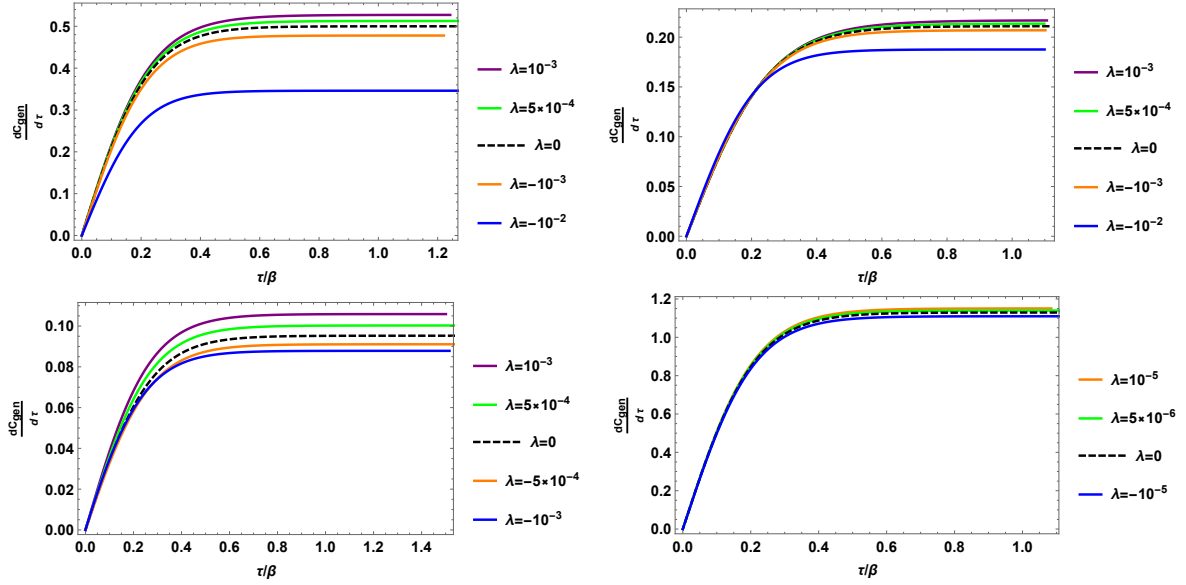


Figure 14. The growth rate $\frac{dC_{\text{gen}}}{dr}$ as a function of τ/β for different values of $\lambda \neq 0$: *Top Left*) $d = 2$, $\theta = 0$ and $z = 1$. *Top Right*) $d = 3$, $\theta = 1$ and $z = 2$. *Down Left*) $d = 4$, $\theta = 2$ and $z = 3$. *Down Right*) $d = 5$, $\theta = -1$ and $z = 2$. We also plotted it for the case $\lambda = 0$, i.e. volume-complexity, which is indicated by the dashed black curve. We set $L = r_h = G_N = V_d = 1$ and $r_F = 0.5$.

numerically plotted the growth rate for different values of λ in Figure 14.

It should be pointed out that to have the so-called linear growth rate at late times, one has to choose λ properly such that the effective potential $\hat{U}(w)$ has a *local maximum inside the horizon*. In ref. [48], it was argued that for small values of λ , such maximum always exists.¹⁹ In our case, depending on the value of d, θ, z and λ , the effective potential might have:

1. no maxima neither inside nor outside the horizon (See Figure 15)
2. one maximum inside the horizon and no maximum outside the horizon (See Figure 16)
3. no maximum inside the horizon and one maximum outside the horizon (See Figure 17)
4. one maximum inside the horizon and another one outside the horizon (See Figure 18)
5. two maxima outside the horizon (See Figure 19).

It is interesting to know what happens to the growth rate when there is no maximum inside the horizon.²⁰ To address this question, in Figures²¹ 15, 16, 17, 18 and 19 we considered an example for each of the above cases, respectively. In Figure 15, we considered the case $d = 2, \theta = 0, z = 1$ and $\lambda = 5 \times 10^{-3} > \frac{1}{12}\lambda_{\text{crit},1}$. In this case, according to Table 4, there is no maximum inside the horizon, and hence the growth rate does not show the so-called linear growth at late times. In the left panel of Figure 15, we plotted the effective potential which shows that there are no maxima neither inside nor outside the horizon. In the middle panel of the figure, we plotted τ as a function of $s_{\text{min}} = \frac{r_{\text{min}}}{r_h}$. It is observed that when s_{min} is large enough, for each value of τ there are two values of r_{min} . In the right panel of the figure, we plotted $\frac{dC_{\text{gen}}}{d\tau}$ as a function of τ/β . There are two branches which are indicated in orange and blue. Therefore, for each value of τ , there are two values of $\frac{dC_{\text{gen}}}{d\tau}$, and hence two branches for $\frac{dC_{\text{gen}}}{d\tau}$.²² In the middle panel of the figure, the blue curve has a larger value of r_{min} in comparison to the orange curve. Moreover, by looking at Figure 1, as the time increases the endpoints of the extremal surface, e.g. the orange curve in Figure 1, moves upward. In this case, the value of r_{min} decreases and reaches r_f at late times. Next, by looking at the middle panel in Figure 15, it is evident that on the orange curve as τ increases r_{min} increases. On the other hand, on the blue curve, as τ increases, r_{min} decreases. Therefore, the correct values of r_{min} are given by the blue curve in the middle panel. Consequently, it is expected that the correct values of $\frac{dC_{\text{gen}}}{d\tau}$ are given by the blue curve in the right panel. It should also be pointed out that the blue curve for $\frac{dC_{\text{gen}}}{d\tau}$ in the right panel does not show the linear growth rate at late times, and even is faster than linear. It is widely believed that the quantum complexity and hence its gravity dual show a linear growth rate at late times (See for example [3]). Therefore, this case in which the late time behavior is not linear seems not to be physical.

In Figure 16, we considered the case, $d = 3, \theta = 0, z = 3$ and $\lambda = 10^{-2}$. In this case, there is just one maximum w_{fB1} and it is located inside the horizon. The growth rate is linear at late times and its value is given by the value of $\hat{U}(w)$ at w_{fB1} according to eq. (3.23).

¹⁹For an AdS-Schwarzschild black brane, depending on the value of the coupling constant, $\hat{U}(w)$ might have 1) no maxima neither inside nor outside the horizon 2) one maximum inside the horizon 3) one maximum outside the horizon. Refer to Figure 3 in ref. [48].

²⁰We would like to thank the referee for raising this intriguing question. We are also very grateful to Mohsen Alishahiha and Robert Myers for their very helpful discussions in this regard.

²¹In all of the figures, we set $L = r_h = r_F = V_d = G_N = 1$.

²²We would like to thank the referee very much for her/his very helpful comments about the two branches in Figure 15.

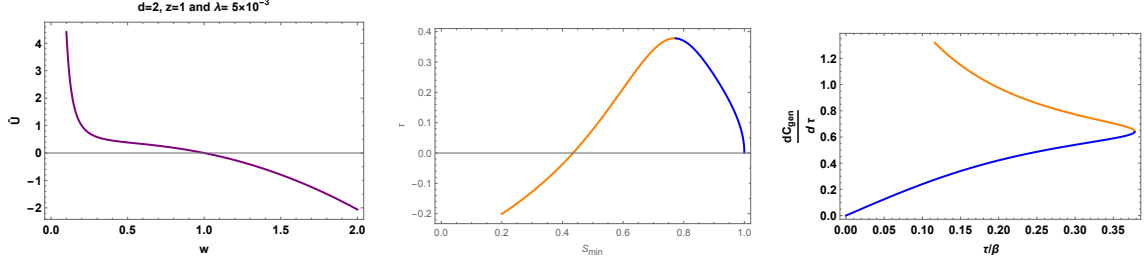


Figure 15. The case $d = 2$, $\theta = 0$, $z = 1$ and $\lambda = 5 \times 10^{-3}$: *Left*) The effective potential as a function of w . For this value of λ there are no maxima neither inside or outside the horizon. *Middle*) τ/β in terms of $s_{\min} = \frac{r_{\min}}{r_h}$. For each value of τ there are two values of r_{\min} . Therefore, it is expected that there are two branches for $\frac{d\mathcal{C}_{\text{gen}}}{d\tau}$ which one of them should be unphysical. The blue curve has larger values of r_{\min} in comparison to the orange one. Moreover, according to Figure 1, as time passes r_{\min} decreases. Therefore, the correct values of r_{\min} are given by the blue curve. *Right*) The growth rate $\frac{d\mathcal{C}_{\text{gen}}}{d\tau}$ in terms of τ/β . There are two branches indicated in blue and orange. The physical branch is the blue curve. It is evident that \mathcal{C}_{gen} does not grow linearly at late times. This is due to the fact that $\lambda > \frac{12}{\lambda_{\text{crit},1}}$, and it does not satisfy the given bound in Table 4.

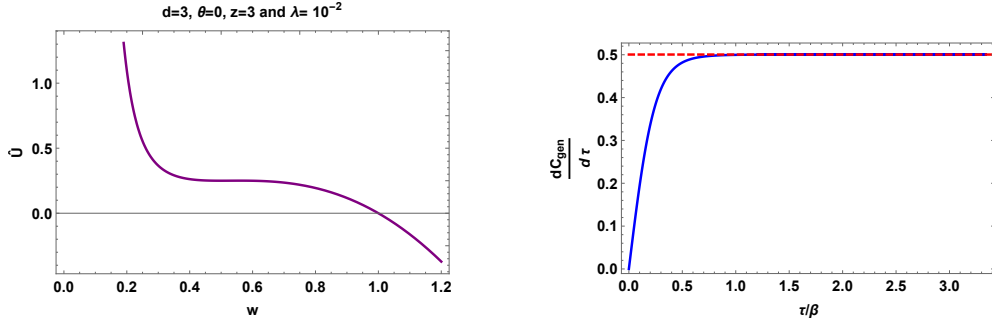


Figure 16. The case $d = 3$, $\theta = 0$, $z = 3$ and $\lambda = 0.01$: *Left*) The effective potential as a function of w . For this value of λ there is just one maximum w_{fB1} . It is located inside the horizon and is the solution to equation $B(\lambda, w) = 0$. *Right*) The growth rate $\frac{d\mathcal{C}_{\text{gen}}}{d\tau}$ in terms of τ/β . The late time growth rate is linear at late times and its value indicated by the red dashed horizontal line is given by eq. (3.23).

In Figure 17, we considered the case $d = 2$, $\theta = 0$, $z = 1$ and $\lambda = -0.2$. In this case, there is just one maximum w_{fA1} which is located outside the horizon. The growth rate is negative and is a decreasing function of τ/β . Therefore, this case is not physical.

In Figure 18, we considered the case $d = 2$, $\theta = 0$, $z = 2$ and $\lambda = -0.3$. In this case, there is a maximum w_{fA2} inside the horizon and another one w_{fB3} outside the horizon. The growth rate at late times is linear and given by the value of $\hat{U}(w)$ at w_{fA2} according to eq. (3.23). It should be pointed out that when there are two maxima, one should choose the maximum which gives a larger value for \mathcal{C}_{gen} .

In Figure 19, we considered the case $d = 4$, $\theta = 0$, $z = 2$ and $\lambda = -0.25$. In this case, there are two

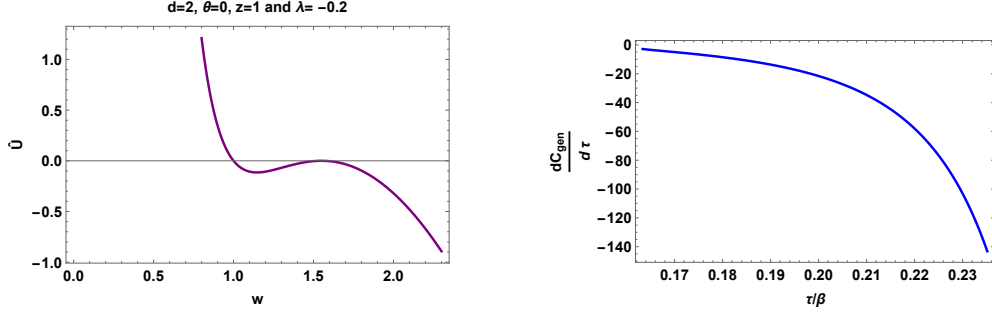


Figure 17. The case $d = 2, \theta = 0, z = 1$ and $\lambda = -0.2$: *Left*) The effective potential as a function of w . For this value of λ there is just one maximum w_{fA1} which is located inside the horizon. *Right*) The growth rate $\frac{dC_{\text{gen}}}{d\tau}$ in terms of τ/β . The late time growth rate is negative and a decreasing function of τ . Notice that since the growth rate is negative this case is not physical.

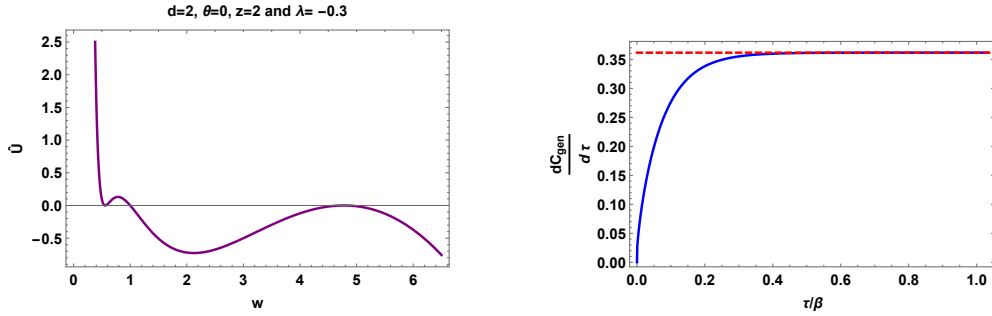


Figure 18. The case $d = 2, \theta = 0, z = 2$ and $\lambda = -0.3$: *Left*) The effective potential as a function of w . For this value of λ , there are two maxima. There is a maximum w_{fA2} inside the horizon which is the solution to equation $A(\lambda, w) = 0$ and there is another one w_{fB3} outside the horizon which is the solution to equation $B(\lambda, w) = 0$. *Right*) The growth rate $\frac{dC_{\text{gen}}}{d\tau}$ in terms of τ/β . The late time growth rate is given by the value of $\hat{U}(w)$ at the maximum w_{fA2} inside the horizon according to eq. (3.23). This value is shown by the horizontal dashed red line. Notice that $\hat{U}(w_{fB3}) = 0$, and hence it gives a zero contribution to eq. (3.23).

maxima $w_{fA1,2}$ which both of them are located outside the horizon. The growth rate at late times is not linear and it is negative. Therefore, this case is not physical.

Therefore, from Figures 15, 16, 17, 18 and 19, one might conclude that only when the coupling constant λ is chosen such that the effective potential has a *maximum inside the horizon*, the growth rate behaves *linearly* at late times. If there is not a maximum inside the horizon, either the growth rate is negative or increases faster than linear at late times. For this reason, throughout the paper we focused on the cases where there is a maximum inside the horizon.

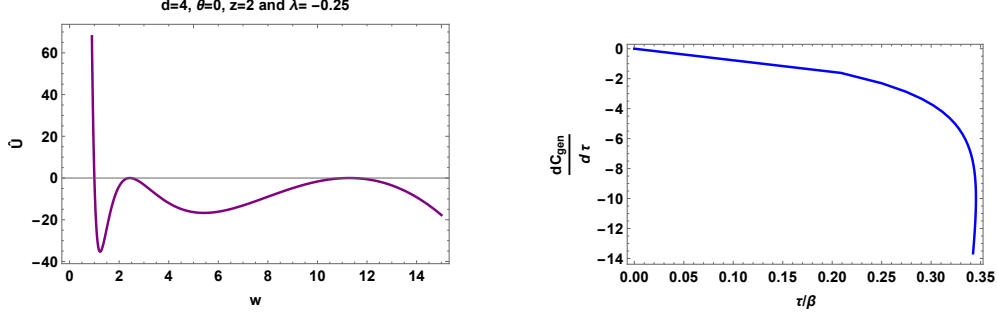


Figure 19. The case $d = 4, \theta = 0, z = 2$ and $\lambda = -0.25$: *Left*) The effective potential as a function of w . For this value of λ , there are two maxima $w_{fA1,2}$ which are located outside the horizon. These are the solutions to equation $A(\lambda, w) = 0$. *Right*) The growth rate $\frac{d\mathcal{C}_{\text{gen}}}{d\tau}$ in terms of τ/β . It is negative and a decreasing function of τ/β , and hence it is not physical.

4 Complexity of Formation

In this section, we calculate the complexity of formation obtained from volume-complexity. In ref. [68], the complexity of formation for a two-sided AdS-black hole was defined as follows

$$\Delta\mathcal{C} = \mathcal{C}^{\text{BH}} - 2\mathcal{C}^{\text{Vac}}, \quad (4.1)$$

where \mathcal{C}^{BH} and \mathcal{C}^{Vac} are the complexity of the two-sided black hole and the corresponding vacuum, respectively. In the above formula, \mathcal{C} can be either volume-complexity [68] or action-complexity [21, 68, 70]. Here, we apply it for \mathcal{C}_V . In this case, the vacuum, i.e. the zero-temperature HV geometry, is given by eq. (2.13). To calculate $\Delta\mathcal{C}_V$, we consider an extremal hypersurface which is anchored at $t_L = t_R = 0$. By symmetry, the extremal hypersurface is a bulk surface for which $t = 0$ (See the magenta straight line in Figure 1). In this case, from eq. (1.4), one simply obtains \mathcal{C}_{gen} of the black brane as follows

$$\mathcal{C}_{\text{gen}} = \frac{2V_d r_F^{\theta_e(d+1)}}{G_N L^d} \int_{r_h}^{r_{\text{max}}} \frac{r^{d_e - \theta_e - 1}}{\sqrt{f(r)}} a(r) dr. \quad (4.2)$$

Next, by setting $\lambda = 0$, one obtains the corresponding volume-complexity

$$\mathcal{C}_V = \frac{2V_d r_F^{\theta_e(d+1)}}{G_N L^d} \int_{r_h}^{r_{\text{max}}^{\text{BB}}} \frac{r^{d_e - \theta_e - 1}}{\sqrt{f(r)}} dr. \quad (4.3)$$

In the following, we consider the two cases $\theta = 0$ and $\theta \neq 0$, separately. It should be pointed out that the radial cutoff r_{max} in the black brane (BB) geometry and the vacuum are different. Therefore, to calculate the complexity of formation in eq. (4.1), one has to find the relation between the two cutoffs $r_{\text{max}}^{\text{BB}}$ and $r_{\text{max}}^{\text{Vac}}$. However, both geometries have the same radial cutoff at $z = \delta$ in the Fefferman-Graham (FG) coordinate. We investigate this connection in Appendix A.

4.1 $\theta = 0$

For the case $\theta = 0$, from eq. (4.3), one obtains

$$\mathcal{C}_V = \frac{2V_d}{G_N d} \left(\frac{r}{L}\right)^d {}_2F_1\left(\frac{1}{2}; -\frac{d}{d+z}, \frac{z}{d+z}; \left(\frac{r_h}{r}\right)^{d+z}\right) \Big|_{r_h}^{r_{\text{max}}^{\text{BB}}}. \quad (4.4)$$

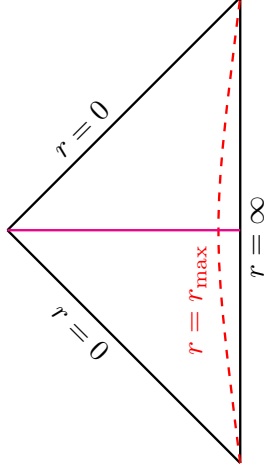


Figure 20. Penrose diagram of the vacuum whose metric is given in eq. (2.13). The red dashed curve is the radial cutoff at $r = r_{\max}$. Moreover, the magenta straight line denotes the extremal hypersurface anchored at $t = 0$ which is applied in the calculation of the complexity of formation.

Next, by plugging eq. (A.18) into the above expression, and expanding it in powers of $\delta \ll 1$, one has

$$\begin{aligned} \mathcal{C}_V &= \frac{2V_d}{G_N} \left[\frac{1}{d} \left(\frac{L}{\delta} \right)^d + \frac{\kappa_0}{8} \left(\frac{r_h}{L} \right)^d + \mathcal{O}(\delta^z) \right] \\ &= \frac{2V_d}{G_N d} \left(\frac{L}{\delta} \right)^d + \kappa_0 S + \mathcal{O}(\delta^z), \end{aligned} \quad (4.5)$$

where S is the thermal entropy given in eq. (2.10). Moreover, κ_0 is a dimensionless constant defined as follows

$$\kappa_0 = \begin{cases} 0 & d = z, \\ -\frac{8\sqrt{\pi}\Gamma(\frac{z}{2+d})}{d\Gamma(\frac{z-d}{2(d+z)})} & d \neq z. \end{cases} \quad (4.6)$$

For large values of d , it approaches a constant

$$\kappa_0 = \frac{4}{z} + \mathcal{O}\left(\frac{1}{d}\right). \quad (4.7)$$

Furthermore, for the case $z = 1$, one has

$$\kappa_0 = \begin{cases} 0 & d = 1, \\ -\frac{8\sqrt{\pi}\Gamma(\frac{1}{d+1})}{d\Gamma(\frac{1-d}{2(d+1)})} = \frac{8\sqrt{\pi}\Gamma(\frac{-d}{d+1})}{(d+1)\Gamma(\frac{-d}{2(d+1)})} & d \neq 1, \end{cases} \quad (4.8)$$

and eq. (4.5) reduces to the volume-complexity of a planar AdS-Schwarzschild black hole (See eq. (5.6) in ref. [68].) On the other hand, for the vacuum, by setting $f(r) = 1$ in eq. (4.3), one has (See Figure 20)

$$\mathcal{C}_V^{\text{Vac}} = \frac{V_d r_F^{\theta_e(d+1)}}{G_N L^d} \int_0^{r_{\max}^{\text{Vac}}} r^{d_e - \theta_e - 1} dr \quad (4.9)$$

$$= \frac{V_d r_F^{\theta_e(d+1)}}{(d_e - \theta_e) G_N L^d} (r_{\max}^{\text{Vac}})^{d_e - \theta_e}. \quad (4.10)$$

For the case $\theta = 0$, it is simplified as follows

$$\mathcal{C}_V^{\text{Vac}} = \frac{V_d}{G_N d} \left(\frac{r_{\max}^{\text{Vac}}}{L} \right)^d. \quad (4.11)$$

Next, by plugging eq. (A.17) into the above equation, one has

$$\mathcal{C}_V^{\text{Vac}} = \frac{V_d}{G_N d} \frac{L^d}{\delta^d}. \quad (4.12)$$

Then by substituting eqs. (4.5) and (4.12) into eq. (4.1), and taking the limit $\delta \rightarrow 0$, one has

$$\Delta \mathcal{C}_V = \mathcal{C}_V^{\text{BB}} - 2 \mathcal{C}_V^{\text{Vac}} = \kappa_0 S. \quad (4.13)$$

Therefore, the UV divergent terms in $\mathcal{C}_V^{\text{BB}}$ and $\mathcal{C}_V^{\text{Vac}}$ cancel each others, and the result is proportional to the thermal entropy S .

4.2 $\theta \neq 0$

For $\theta \neq 0$, from eq. (4.3) it is clear that one has to consider the two cases $d_e \neq \theta_e$ and $d_e = \theta_e$, separately. The reason is that for the former the UV divergent terms are power law and for the latter they are logarithmic.

4.2.1 $d_e \neq \theta_e$

In this case, it is straightforward to check that the integral in eq. (4.3) has no analytical results for arbitrary values of d , θ and z . However, for some cases²³ it can be calculated analytically as follows

$$\mathcal{C}_V = \frac{2V_d r_F^{\theta_e(d+1)}}{G_N (d_e - \theta_e)} \left(\frac{r^{d_e - \theta_e}}{L^d} \right) {}_2F_1 \left(\frac{1}{2}; -\frac{(d_e - \theta_e)}{(d_e + z)}, \frac{z + \theta_e}{d_e + z}; \left(\frac{r_h}{r} \right)^{d_e + z} \right) \Big|_{r_h}^{r_{\max}^{\text{BB}}}. \quad (4.14)$$

Next, by plugging eq. (A.35) into the above expression, and expanding it in powers of $\delta \ll 1$, one has

$$\begin{aligned} \mathcal{C}_V &= \frac{2V_d r_F^{\theta_e(d+1)}}{G_N} \left[\frac{L^{d_e - \theta_e(d+2)}}{(d_e - \theta_e)} \frac{1}{\delta^{d_e - \theta_e}} + \frac{\kappa}{8} \frac{r_h^{d_e - \theta_e}}{L^d} + \mathcal{O}(\delta^{z+\theta_e}) + \dots \right] \\ &= \frac{2V_d}{G_N (d_e - \theta_e)} \left(\frac{r_F}{L} \right)^{\theta_e(d+1)} \left(\frac{L}{\delta} \right)^{d_e - \theta_e} \\ &\quad + \kappa \left(\frac{4\pi L^{z+1}}{(d_e + z) r_F^z} \right)^{-\frac{\theta_e}{z}} S T^{-\frac{\theta_e}{z}} + \mathcal{O}(\delta^{z+\theta_e}) + \dots, \end{aligned} \quad (4.15)$$

²³For example, it can be calculated for the following cases

- $d = 1$ and $\theta = \frac{1}{3}, \frac{2}{3}, \frac{3}{4}, \frac{1}{5}, \frac{2}{5}, \frac{3}{5}, \frac{4}{5}, \frac{1}{6}, \frac{5}{6}, \frac{1}{7}, \frac{2}{7}, \frac{3}{7}, \frac{4}{7}, \frac{5}{7}, \frac{6}{7}, \frac{1}{8}, \frac{3}{8}, \frac{5}{8}, \frac{7}{8}, \frac{1}{9}, \dots$
- $d = 2$ and $\theta = \frac{3}{2}, \frac{5}{3}, \frac{7}{4}, \frac{6}{5}, \frac{7}{5}, \frac{8}{5}, \frac{9}{5}, \frac{7}{6}, \frac{11}{6}, \frac{8}{7}, \frac{9}{7}, \frac{10}{7}, \frac{11}{7}, \frac{12}{7}, \frac{13}{7}, \frac{9}{8}, \frac{11}{8}, \dots$
- $d = 3$ and $\theta = \frac{5}{2}, \frac{7}{3}, \frac{8}{3}, \frac{11}{4}, \frac{11}{5}, \frac{12}{5}, \frac{14}{5}, \frac{13}{6}, \frac{17}{6}, \frac{15}{7}, \frac{16}{7}, \frac{18}{7}, \frac{19}{7}, \frac{20}{7}, \frac{17}{8}, \frac{19}{8}, \dots$

Moreover, for the following cases, $\{d = 1, \theta = \frac{1}{4}\}, \{d = 2, \theta = \frac{1}{3}, -3\}, \{d = 3, \theta = \frac{9}{8}, \frac{15}{8}\}$, volume-complexities are again given by hypergeometric functions. However, they cannot be written in the form given in eq. (4.14).

For these cases, one still has $\Delta \mathcal{C}_V \propto S T^{-\frac{\theta_e}{z}}$.

where ²⁴

$$\kappa = -\frac{8\sqrt{\pi}\Gamma\left(\frac{z+\theta_e}{d_e+z}\right)}{(d_e-\theta_e)\Gamma\left(\frac{z-d_e+2\theta_e}{2(d_e+z)}\right)}. \quad (4.16)$$

Moreover, for large values of d , it approaches a constant

$$\kappa = \frac{4}{z} + \mathcal{O}\left(\frac{1}{d}\right). \quad (4.17)$$

On the other hand, for the vacuum, by plugging eq. (A.34) into eq. (4.10), one arrives at

$$\begin{aligned} \mathcal{C}_V^{\text{Vac}} &= \frac{V_d r_F^{\theta_e(d+1)}}{(d_e-\theta_e)G_N L^d} (r_{\text{max}}^{\text{Vac}})^{d_e-\theta_e} \\ &= \frac{V_d r_F^{\theta_e(d+1)}}{(d_e-\theta_e)G_N} \frac{L^{d_e-\theta-2\theta_e}}{\delta^{d_e-\theta_e}}. \end{aligned} \quad (4.18)$$

Next, by plugging eqs. (4.15) and (4.18) into eq. (4.1), and taking the limit $\delta \rightarrow 0$, one obtains

$$\Delta\mathcal{C}_V = \kappa \left(\frac{4\pi L^{z+1}}{(d_e+z)r_F^z} \right)^{-\frac{\theta_e}{z}} ST^{-\frac{\theta_e}{z}} = \xi ST^{-\frac{\theta_e}{z}}, \quad (4.19)$$

where

$$\xi = \kappa \left(\frac{4\pi L^{z+1}}{(d_e+z)r_F^z} \right)^{-\frac{\theta_e}{z}}. \quad (4.20)$$

Therefore, similar to the case $\theta = 0$, the UV divergent terms in $\mathcal{C}_V^{\text{BB}}$ and $\mathcal{C}_V^{\text{Vac}}$ cancel each others exactly. Moreover, $\Delta\mathcal{C}_V$ is proportional to $ST^{-\frac{\theta_e}{z}}$. Furthermore, for $\theta = 0$, eq. (4.19) reduces to eq. (4.13).

4.2.2 $d_e = \theta_e$

For $d_e = \theta_e$ or equivalently

$$\theta = \frac{d^2}{d+1}, \quad (4.21)$$

by applying eqs. (4.3) and (A.35), one easily obtains

$$\begin{aligned} \mathcal{C}_V &= \frac{2V_d r_F^d}{G_N L^d} \int_{r_h}^{r_{\text{max}}^{\text{BB}}} \frac{1}{r\sqrt{f(r)}} dr \\ &= \frac{4V_d}{G_N(z+\theta_e)} \left(\frac{r_F}{L}\right)^d \tanh^{-1} \sqrt{1 - \left(\frac{r_h}{r_{\text{max}}^{\text{BB}}}\right)^{z+\theta_e}} \\ &= \frac{2V_d}{G_N(d+z(d+1))} \left(\frac{r_F}{L}\right)^d \log \left[2^{2(d+1)} \left(\frac{L^2}{r_h \delta}\right)^{d+z(d+1)} \right] + \mathcal{O}(\delta^{z+\theta_e}). \end{aligned} \quad (4.22)$$

²⁴Notice that when $\theta = 0$, κ reduces to κ_0 for the case $d \neq z$.

Therefore, the UV divergent term is logarithmic in this case. On the other hand, for the vacuum, from eq. (4.9), one has

$$\begin{aligned}\mathcal{C}_V^{\text{Vac}} &= \frac{V_d r_F^d}{G_N L^d} \int_{\epsilon}^{r_{\text{max}}^{\text{Vac}}} \frac{dr}{r} = \frac{V_d r_F^d}{G_N L^d} \log\left(\frac{r_{\text{max}}^{\text{Vac}}}{\epsilon}\right) \\ &= \frac{V_d r_F^d}{G_N L^d} \log\left(\frac{L^2}{\epsilon \delta}\right),\end{aligned}\tag{4.23}$$

where $\bar{\epsilon} \rightarrow 0$ is an IR cutoff. Next, from eqs. (4.22) and (4.23), one can find $\Delta\mathcal{C}_V$ as follows

$$\begin{aligned}\Delta\mathcal{C}_V &= \frac{2V_d}{G_N} \left(\frac{r_F}{L}\right)^d \log\left(\frac{2^{\frac{2}{z+\theta}\epsilon}}{r_h}\right) \\ &= \frac{2V_d}{G_N} \left(\frac{r_F}{L}\right)^d \log\left(\frac{4^{\frac{d_c}{4e+\theta z}} \epsilon^{d_c} V_d r_F^\theta}{4G_N L^d S}\right).\end{aligned}\tag{4.24}$$

It is observed that the logarithmic UV divergent terms in eqs. (4.22) and (4.23) are canceled. Moreover, $\Delta\mathcal{C}_V$ depends on $\log S$.

5 Discussion

In this paper, we studied the generalized volume-complexity \mathcal{C}_{gen} which is an extension of volume-complexity for a two-sided uncharged HV black brane in $d+2$ dimensions. We considered the case where the two functionals F_1 and F_2 are equal to each other such that $F_1 = F_2 = 1 + \lambda C^2$. Here C^2 is the square of the Weyl tensor of the background and λ is a dimensionless coupling constant. We investigated the two cases $\lambda = 0$ and $\lambda \neq 0$, separately. For both cases, it was proved that the growth rate of generalized volume-complexity at late times, i.e. $\lim_{\tau \rightarrow \infty} \frac{d\mathcal{C}_{\text{gen}}}{d\tau}$, is determined by the maxima of the effective potential $\hat{U}(r)$ which are located inside the horizon (See eq. (3.23)). Therefore, we also investigated these maxima.

For the case, $\lambda = 0$, \mathcal{C}_{gen} reduces to the volume-complexity \mathcal{C}_V in the CV proposal. In this case, the effective potential $\hat{U}(w)$ has a simple maximum inside the horizon. Therefore, one is able to analytically calculate the late time growth rate (See eq. (3.29)). We also numerically calculated the growth rate $\frac{d\mathcal{C}_V}{d\tau}$ of volume-complexity (See Figures 2, 3 and 4) for different values of d , θ and z . It was observed that it always saturates to a constant value at late times and reaches this value from *below*. Furthermore, it is an increasing function of d , and is a decreasing function of the dynamical exponent z (See Figures 2 and 3). However, it is neither an increasing nor a decreasing function of θ (See Figure 4).

For the case $\lambda \neq 0$, we calculated numerically the growth rate $\frac{d\mathcal{C}_{\text{gen}}}{d\tau}$ of generalized volume-complexity (See Figures 11, 12, 13 and 14) for different values of d , θ , z and λ . It was observed that for appropriate ranges of λ , it saturates to a constant value at late times and reaches this value from *below*. Furthermore, it is neither an increasing nor a decreasing function of d and z (See Figures 11 and 12). However, it is an increasing function of the exponent θ (See Figure 13). Moreover, it is an increasing function of λ (See Figure 14).

On the other hand, for the case $\lambda \neq 0$, we also examined the maxima of $\hat{U}(w)$. It was observed that for arbitrary values of d , θ and z , there are no analytical solutions to equation $\hat{U}''(w) = 0$. However, for the following cases one can find analytical solutions: 1) $\theta = 0$ and arbitrary values of d and z , 2) $d = 2$, $\theta = 1$ and $z = 1$. It was observed that for the case $\theta = 0$, i.e. Lifshitz black branes, there are three possible local maxima w_{fA1} , w_{fA2} and w_{fB} depending on the value of the coupling constant λ .

These values were reported in Tables 1, 2, 3 and 4. The maxima at $w = w_{fA1,2}$ are always located outside the horizon (See Figures 5 and 6), and hence have no significance. On the other hand, the maximum at $w = w_{fB}$ is located either inside or outside the horizon depending on the value of λ (See Figures 7 and 8). Moreover, for the case $d = 2$, $\theta = 1$ and $z = 1$, the appropriate range of λ is given by eq. (3.55). It should be pointed out that for $\theta = 0$ and $z = 1$, the HV black brane becomes a planar AdS-Schwarzschild black hole and all of our results reduce to those reported in ref. [48].

On the other hand, we calculated the growth rate of generalized complexity in Appendix B for the case where $F_1 = F_2$ and they are a linear combination of the Ricci scalar, square of the Ricci tensor and square of the Riemann tensor (See eq. B.1). It was observed that by choosing the coupling constants $\lambda_{1,2,3}$ properly such that the effective potential has a maximum inside the horizon, the growth rate again has a linear behavior at late times.

Furthermore, we calculated the complexity of formation $\Delta\mathcal{C}_V$ obtained from volume-complexity. We observed that the UV divergent terms in \mathcal{C}_V both for the black brane and the vacuum geometries cancel each other exactly. Therefore, in the limit $\delta \rightarrow 0$, where δ is the radial cutoff in the Fefferman-Graham coordinate, $\Delta\mathcal{C}_V$ is finite. For the case $\theta = 0$, it is proportional to the thermal entropy S of the black brane (See eq. (4.13)). On the other hand, for the case $\theta \neq 0$ and $d_e \neq \theta_e$, it can be analytically calculated for some values of d and θ . For these values, it was observed that $\Delta\mathcal{C}_V$ is proportional to $ST^{-\frac{\theta_e}{z}}$, where T is the temperature of the black brane (See eq. (4.19)). Moreover, for the case $\theta \neq 0$ and $d_e = \theta_e$, it depends on $\log S$ (See eq. (4.24)). It should be pointed out that for AdS black holes, one has $\Delta\mathcal{C}_V \propto S$ [68]. Therefore, the behavior of $\Delta\mathcal{C}_V$ for the case $\theta \neq 0$ is very intriguing. In particular, the logarithmic behavior for the case $d_e \neq \theta_e$, and it would be very interesting to further investigate it.

Eventually, in ref. [21], the effect of nonzero charge on volume-complexity \mathcal{C}_V was explored for charged planar AdS black holes. It was observed that for a given temperature, by increasing the charge, the growth rate of \mathcal{C}_V decreases. It would be interesting to investigate the effect of charge on generalized volume-complexity \mathcal{C}_{gen} by considering charged HV or AdS black holes. Moreover, it would be also interesting to study different scalar functional F_1 of the background curvature as well as cases in which the functionals F_1 and F_2 are not equal to each other. Another interesting direction to pursue is to extend these calculations to the HV black hole solutions found in ref. [130] or Kerr-AdS black holes whose volume-complexity were recently studied in ref. [69].

Acknowledgment

We would like to thank Mohsen Alishahiha very much for his support and illuminating discussions during this work. We would also like to thank Mohsen Alishahiha, Robert Myers and Ali Naseh very much for their very valuable comments on the draft. We are also very grateful to Ghadir Jafari for helpful discussions. The work of FO is supported by the School of Physics at IPM and Iran Science Elites Federation (ISEF).

Appendix

A Connection between the Radial Cutoffs

In this section, we investigate the connection between the radial cutoffs $r_{\text{max}}^{\text{BB}}$ and $r_{\text{max}}^{\text{Vac}}$. To this end, we proceed in the same manner as Appendix A in ref. [68], and work in the Fefferman-Graham (FG) coordinate. We assume that both the black brane geometry and the vacuum have the same radial

cutoff at $z = \delta$ in the FG coordinate. We write the metric (2.4) in the FG coordinate

$$ds^2 = \frac{L^2}{z^2} (dz^2 + g_{ij}(z, x^i) dx^i dx^j), \quad (\text{A.1})$$

where $g_{ij}(z, x^i)$ is the boundary metric. For an asymptotically AdS spacetime the coordinates z and r are connected as follows²⁵

$$z = \frac{L^2}{r} + \frac{a_1}{r^2} + \cdots + \frac{a_d}{r^{d+2}} + \frac{a_{d+2}}{r^{d+3}} + \cdots, \quad (\text{A.2})$$

Therefore, at leading order one has $z = \frac{L^2}{r}$. Moreover, the first non-zero coefficient that is different between the black hole geometry and the vacuum is a_d [68]. In the following, we first investigate how the above formula is changed for a HV black brane. Next, we find the connection between $r_{\text{max}}^{\text{BB}}$ and $r_{\text{max}}^{\text{Vac}}$. Asking for the radial part of the black brane metric in eqs. (2.4) and (A.1) to be equal to each other, one has

$$\frac{dz}{z} = -\frac{r^{\theta_e}}{r^{\theta_e+1} \sqrt{f(r)}} dr. \quad (\text{A.3})$$

In the following, we consider the two cases $\theta = 0$ and $\theta \neq 0$, separately.

A.1 $\theta = 0$

For very large r , one has

$$f(r) \approx 1, \quad (\text{A.4})$$

and hence by taking the integral of eq. (A.3), one obtains

$$\log z = -\log r + \tilde{c}, \quad (\text{A.5})$$

or equivalently

$$z = \frac{L^2}{r}. \quad (\text{A.6})$$

It should be pointed out that we choose the integration constant such that at leading order, one has $z = \frac{L^2}{r}$ (See also [68]). Moreover, to find the subleading corrections to eq. (A.6), one can expand $f(r)$ in powers of r in eq. (A.3) and taking the integrals on both sides. It is straightforward to see that

$$z = \frac{L^2}{r} + \frac{a_1}{r^{d+z+1}} + \frac{a_2}{r^{2(d+z)+1}} + \frac{a_3}{r^{3(d+z)+1}} + \cdots. \quad (\text{A.7})$$

Therefore, at $z = \delta$, one can write δ in terms of r_{max} as follows

$$\delta = \frac{L^2}{r_{\text{max}}} + \frac{a_1}{r_{\text{max}}^{d+z+1}} + \frac{a_2}{r_{\text{max}}^{2(d+z)+1}} + \frac{a_3}{r_{\text{max}}^{3(d+z)+1}} + \cdots. \quad (\text{A.8})$$

Now one can invert the above formula and write r_{max} in terms of δ

$$r_{\text{max}} = \frac{L^2}{\delta} + \tilde{a}_1 \delta^{d+z-1} + \tilde{a}_2 \delta^{2(d+z)-1} + \cdots. \quad (\text{A.9})$$

²⁵Notice that we work in $d+2$ dimensions. Moreover, for $z \rightarrow 0$, one has $r \rightarrow \infty$. Therefore, one can write an expansion for z in inverse powers of r .

Next, we find the connection between r_{\max}^{BB} and r_{\max}^{Vac} . By taking the integral on the left hand side of eq. (A.3), one has

$$\log \frac{\delta}{L^2} = \log \int^{\delta} \frac{dz}{z} = - \int^{r_{\max}} \frac{dr}{r\sqrt{f(r)}}. \quad (\text{A.10})$$

It should be pointed out that one can apply eq. (A.10), both for the black brane and the vacuum geometries. Having this in mind that the radial cutoff δ in the FG coordinate is the same for both geometries, and subtracting eq. (A.10) for both of them, one obtains

$$0 = \int^{r_{\max}^{\text{BB}}} \frac{dr}{r\sqrt{f(r)}} - \int^{r_{\max}^{\text{Vac}}} \frac{dr}{r}. \quad (\text{A.11})$$

Then, we assume that (See also [68])

$$r_{\max}^{\text{BB}} = r_{\max}^{\text{Vac}} + \delta r_{\max}. \quad (\text{A.12})$$

By plugging the above equation into the first integral in eq. (A.11), one can make the following approximation at leading order in δ and r_{\max}^{Vac}

$$\begin{aligned} \int^{r_{\max}^{\text{BB}}} \frac{dr}{r\sqrt{f(r)}} &= \int^{r_{\max}^{\text{Vac}} + \delta r_{\max}} \frac{dr}{r\sqrt{f(r)}} \\ &= \int^{r_{\max}^{\text{Vac}}} \frac{dr}{r\sqrt{f(r)}} + \frac{1}{r\sqrt{f(r)}} \Big|_{r_{\max}^{\text{Vac}} + \delta r_{\max}}^{\delta r_{\max}} \\ &= \int^{r_{\max}^{\text{Vac}}} \frac{dr}{r\sqrt{f(r)}} + \frac{1}{r_{\max}^{\text{Vac}}} (r_{\max}^{\text{BB}} - r_{\max}^{\text{Vac}}), \end{aligned} \quad (\text{A.13})$$

where we applied eq. (A.12) in the last line. Next, by substituting the above equation into eq. (A.11), one arrives at

$$\begin{aligned} \frac{1}{r_{\max}^{\text{Vac}}} (r_{\max}^{\text{BB}} - r_{\max}^{\text{Vac}}) &= \int^{r_{\max}^{\text{Vac}}} \left(1 - \frac{1}{\sqrt{f(r)}} \right) \frac{dr}{r} \\ &= -\frac{r_h^{d+z}}{2} \int^{r_{\max}} \frac{dr}{r^{d+z+1}} + \dots \\ &\simeq \frac{r_h^{d+z}}{2(d+z)} \left(\frac{1}{r_{\max}^{\text{Vac}}} \right)^{d+z} + \dots \end{aligned} \quad (\text{A.14})$$

From the above equation, one easily obtains

$$r_{\max}^{\text{BB}} = r_{\max}^{\text{Vac}} + \frac{r_h^{d+z}}{2(d+z)} \left(\frac{1}{r_{\max}^{\text{Vac}}} \right)^{d+z-1} + \dots \quad (\text{A.15})$$

Next, we find the connection between r_{\max}^{Vac} and δ . From eq. (A.10), one can find

$$\log \frac{\delta}{L^2} = - \int^{r_{\max}^{\text{Vac}}} \frac{dr}{r} = - \log r + \tilde{c}, \quad (\text{A.16})$$

or equivalently,

$$r_{\max}^{\text{Vac}} = \frac{L^2}{\delta}. \quad (\text{A.17})$$

Therefore, by plugging eq. (A.17) into eq. (A.15), one can write

$$r_{\max}^{\text{BB}} = \frac{L^2}{\delta} + \frac{r_h^{d+z}}{2(d+z)L^{2(d+z-1)}}\delta^{d+z-1} + \dots \quad (\text{A.18})$$

Notice that for $z = 1$, it reduces to eq. (A.13) in ref. [68] for a planar AdS-Schwarzschild black hole in $d + 2$ dimensions as it was expected.

A.2 $\theta \neq 0$

For very large r , one again has $f(r) \approx 1$, and hence

$$\log \frac{\delta}{L^2} = \frac{1}{\theta_e} \left(\frac{r_F}{r_{\max}} \right)^{\theta_e}, \quad (\text{A.19})$$

or equivalently,

$$z = L^2 e^{\frac{1}{\theta_e} \left(\frac{r_F}{r_{\max}} \right)}. \quad (\text{A.20})$$

Notice that from eq. (A.19) for $\theta > 0$ when $r_{\max} \rightarrow \infty$, one has $\delta \rightarrow L^2$. Moreover, for $\theta < 0$ when $r_{\max} \rightarrow \infty$, one has $\delta \rightarrow \infty$. These results are not consistent with the fact that for $r_{\max} \rightarrow \infty$, one must have $\delta \rightarrow 0$. To remedy the issue, we apply the following ansatz for the metric in the FG coordinate

$$ds^2 = \frac{L^2}{z^2} \left(\frac{z_F}{z} \right)^{-2\theta_e} (dz^2 + g_{ij}(z, x^i) dx^i dx^j). \quad (\text{A.21})$$

Notice that for $\theta = 0$, eq. (A.21) reduces to eq. (A.1). Asking for the radial elements in eqs. (2.4) and (A.21) to be equal to each other, changes eq. (A.3) as follows

$$\frac{dz}{z_F^{\theta_e} z^{1-\theta_e}} = -\frac{r_F^{\theta_e}}{r^{1+\theta_e} \sqrt{f(r)}} dr. \quad (\text{A.22})$$

Next, by expanding the blackening factor $f(r)$ in powers of r and taking the integrals on both sides of eq. (A.22), one arrives at

$$z^{\theta_e} = (r_F z_F)^{\theta_e} \left[\frac{1}{r^{\theta_e}} + \frac{\theta_e r_h^{d_e+z}}{2(d_e+z+\theta_e)} \frac{1}{r^{d_e+z+\theta_e}} + \frac{3\theta_e r_h^{2(d_e+z)}}{8(2(d_e+z)+\theta_e)} \frac{1}{r^{2(d_e+z)+\theta_e}} \right. \\ \left. + \frac{5\theta_e r_h^{3(d_e+z)}}{16(3(d_e+z)+\theta_e)} \frac{1}{r^{3(d_e+z)+\theta_e}} + \dots \right], \quad (\text{A.23})$$

which can be recast in the following form

$$z = \frac{L^2}{r} + \frac{a_1}{r^{d_e+z+1}} + \frac{a_2}{r^{2(d_e+z)+1}} + \frac{a_3}{r^{3(d_e+z)+1}} + \dots \quad (\text{A.24})$$

It should be pointed out that in eq. (A.23) we set the integration constant to zero. Moreover, we assume that $z_F = \frac{L^2}{r_F}$. Therefore, at $z = \delta$, one can write δ in terms of r_{\max} as follows

$$\delta = \frac{L^2}{r_{\max}} + \frac{a_1}{r_{\max}^{d_e+z+1}} + \frac{a_2}{r_{\max}^{2(d_e+z)+1}} + \frac{a_3}{r_{\max}^{3(d_e+z)+1}} + \dots \quad (\text{A.25})$$

Now, one can invert the above formula and write r_{\max} in terms of δ as follows

$$r_{\max} = \frac{L^2}{\delta} + \tilde{a}_1 \delta^{d_e+z-1} + \tilde{a}_2 \delta^{2(d_e+z)-1} + \dots \quad (\text{A.26})$$

Then, we find the connection between r_{\max}^{BB} and r_{\max}^{Vac} . By taking the integral on the left hand side of eq. (A.22), one has

$$\frac{1}{\theta_e} \left(\frac{\delta}{z_F} \right)^{\theta_e} = \frac{1}{z_F^{\theta_e}} \int^{\delta} \frac{dz}{z^{1-\theta_e}} = -r_F^{\theta_e} \int^{r_{\max}} \frac{dr}{r^{1+\theta_e} \sqrt{f(r)}}. \quad (\text{A.27})$$

As mentioned before, the cutoff δ in the FG coordinate is the same both for the black brane and the vacuum geometries. Therefore, by subtracting eq. (A.27) for both geometries, one obtains

$$0 = \int^{r_{\max}^{\text{BB}}} \frac{dr}{r^{1+\theta_e} \sqrt{f(r)}} - \int^{r_{\max}^{\text{Vac}}} \frac{dr}{r^{1+\theta_e}}. \quad (\text{A.28})$$

Next, by plugging eq. (A.12) into the first integral in eq. (A.28), one can make the following approximation to the integral at leading order in δ and r_{\max}^{Vac}

$$\begin{aligned} \int^{r_{\max}^{\text{BB}}} \frac{dr}{r^{1+\theta_e} \sqrt{f(r)}} &= \int^{r_{\max}^{\text{Vac}}} \frac{dr}{r^{1+\theta_e} \sqrt{f(r)}} + r_{\max} \delta \left(\frac{1}{r^{1+\theta_e} \sqrt{f(r)}} \right) \Big|_{r_{\max}^{\text{Vac}} + \delta}^{r_{\max}^{\text{BB}}} \\ &= \int^{r_{\max}^{\text{Vac}}} \frac{dr}{r^{1+\theta_e} \sqrt{f(r)}} + \frac{1}{(r_{\max}^{\text{Vac}})^{1+\theta_e}} (r_{\max}^{\text{BB}} - r_{\max}^{\text{Vac}}). \end{aligned} \quad (\text{A.29})$$

Then, by substituting the above equation into eq. (A.28), and expanding the blackening factor in powers of r , one has

$$\begin{aligned} \frac{1}{(r_{\max}^{\text{Vac}})^{1+\theta_e}} (r_{\max}^{\text{BB}} - r_{\max}^{\text{Vac}}) &\simeq \int^{r_{\max}^{\text{Vac}}} \left(1 - \frac{1}{\sqrt{f(r)}} \right) \frac{dr}{r^{1+\theta_e}} \\ &= -\frac{r_h^{d_e+z}}{2} \int^{r_{\max}^{\text{Vac}}} \frac{dr}{r^{d_e+z+\theta_e+1}} + \dots \\ &= \frac{r_h^{d_e+z}}{2(d_e+z+\theta_e)} \left(\frac{1}{r_{\max}^{\text{Vac}}} \right)^{d_e+z+\theta_e} + \dots \end{aligned} \quad (\text{A.30})$$

From the above equation, one easily obtains

$$r_{\max}^{\text{BB}} = r_{\max}^{\text{Vac}} + \frac{r_h^{d_e+z}}{2(d_e+z+\theta_e)} \left(\frac{1}{r_{\max}^{\text{Vac}}} \right)^{d_e+z-1} + \dots \quad (\text{A.31})$$

Now, we find the connection between δ and r_{\max}^{Vac} . For the vacuum one has $f(r) = 1$, and from eq. (A.27), one arrive at

$$\frac{1}{\theta_e} \left(\frac{\delta}{z_F} \right)^{\theta_e} = \frac{1}{z_F^{\theta_e}} \int^{\delta} \frac{dz}{z^{1-\theta_e}} = -r_F^{\theta_e} \int^{r_{\max}^{\text{Vac}}} \frac{dr}{r^{1+\theta_e}}. \quad (\text{A.32})$$

By taking the integral on the right hand side of the above equation, one finds

$$\delta = \frac{r_F z_F}{r_{\max}^{\text{Vac}}}, \quad (\text{A.33})$$

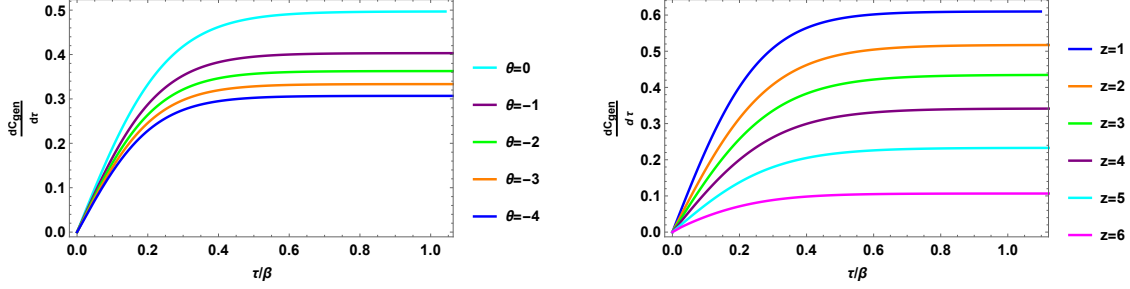


Figure 21. The growth rate $\frac{d\mathcal{C}_{\text{gen}}}{d\tau}$ as a function of τ/β for $a(r) = 1 + \lambda_1 L^4 R$ and different values of d , θ and z : *Left*) $d = 1$, $z = 1$ and $\lambda_1 = 10^{-3}$. *Right*) $d = 2$, $\theta = 1$ and $\lambda_1 = 10^{-2}$.

where we set the integration constant to zero again. Moreover, by setting $z_F = \frac{L^2}{r_F}$, one can rewrite eq. (A.33) as follows

$$r_{\text{max}}^{\text{Vac}} = \frac{L^2}{\delta}. \quad (\text{A.34})$$

At the end, by plugging eq. (A.34) into eq. (A.31), one has

$$r_{\text{max}}^{\text{BB}} = \frac{L^2}{\delta} + \frac{r_h^{d_e+z}}{2(d_e+z+\theta_e)L^{2(d_e+z-1)}}\delta^{d_e+z-1} + \dots. \quad (\text{A.35})$$

B Other Higher Derivative Functionals $F_{1,2}(g_{\mu\nu}; X^\mu(\sigma))$

In this appendix, we briefly examine other extensions of the generalized volume-complexity where one has ²⁶

$$F_1(g_{\mu\nu}; X^\mu(\sigma)) = F_2(g_{\mu\nu}; X^\mu(\sigma)) =$$

$$a(r) = 1 + L^4 (\lambda_1 R + \lambda_2 R_{\mu\nu} R^{\mu\nu} + \lambda_3 R_{\mu\nu\rho\sigma} R^{\mu\nu\rho\sigma}). \quad (\text{B.1})$$

In this case, eqs. (3.3) to (3.16) and eqs. (3.18) to (3.24) are still valid. However, one needs to replace the old $a(r)$ in eq. (3.4) with the new one in eq. (B.1). It is also evident that in this case the effective potential is also changed. Since finding the closed form of $\hat{U}(w)$ for arbitrary values of d, θ and z is very complicated, we do not write it down here. However, it is easy to find it for each value of these parameters. In figures 21, 22 and 23 ²⁷ we plotted numerically the growth rate of \mathcal{C}_{gen} for the following cases, respectively

- $\lambda_1 \neq 0$ and $\lambda_{2,3} = 0$
- $\lambda_2 \neq 0$ and $\lambda_{1,3} = 0$
- $\lambda_3 \neq 0$ and $\lambda_{1,2} = 0$.

Moreover, in Figure 24, we plotted the growth rate for the case $\lambda_{1,2,3} \neq 0$. In all figures, it is evident that the growth rate of \mathcal{C}_{gen} at late times is linear in time, if one chooses $\lambda_{1,2,3}$ such that $\hat{U}(w)$ has a maximum inside the horizon. Therefore, all of the corrections to volume-complexity in eq. (B.1) behave universally at late times.

²⁶We would like to thank the referee very much for her/his helpful suggestions to do these calculations.

²⁷In these figure, we set $L = r_h = r_F = G_N = V_d = 1$.

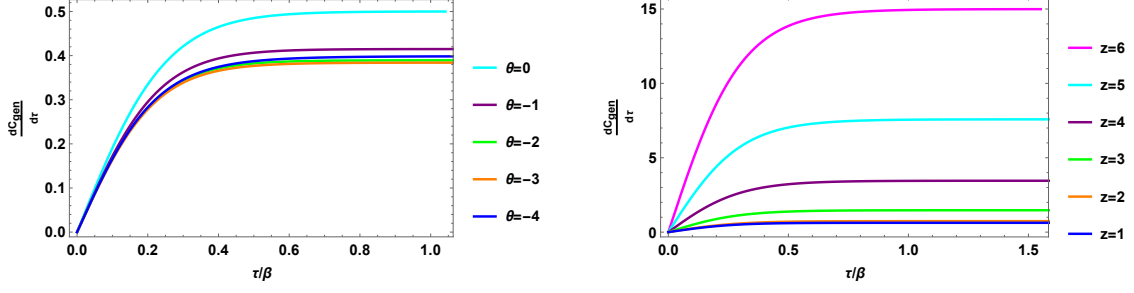


Figure 22. The growth rate $\frac{dC_{\text{gen}}}{d\tau}$ as a function of τ/β for $a(r) = 1 + \lambda_2 L^4 R_{\mu\nu} R^{\mu\nu}$ and different values of d , θ and z : *Left*) $d = 1$, $z = 1$ and $\lambda_2 = 10^{-5}$. *Right*) $d = 2$, $\theta = 1$ and $\lambda_2 = 10^{-2}$.

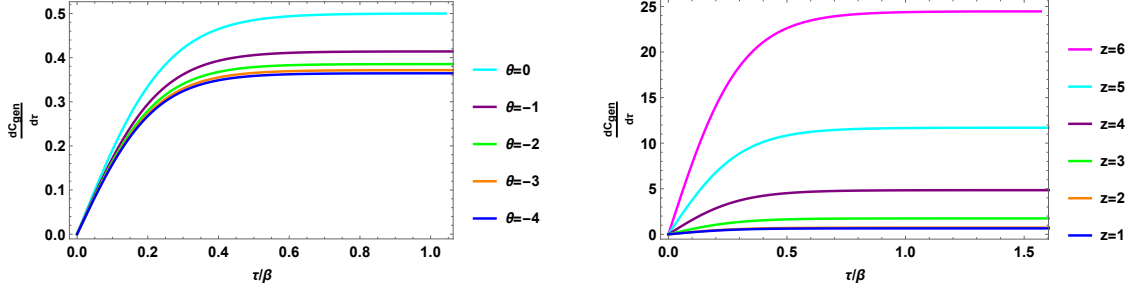


Figure 23. The growth rate $\frac{dC_{\text{gen}}}{d\tau}$ as a function of τ/β for $a(r) = 1 + \lambda_3 L^4 R_{\mu\nu\rho\sigma} R^{\mu\nu\rho\sigma}$ and different values of d , θ and z : *Left*) $d = 1$, $z = 1$ and $\lambda_3 = 10^{-6}$. *Right*) $d = 2$, $\theta = 1$ and $\lambda_3 = 10^{-2}$.

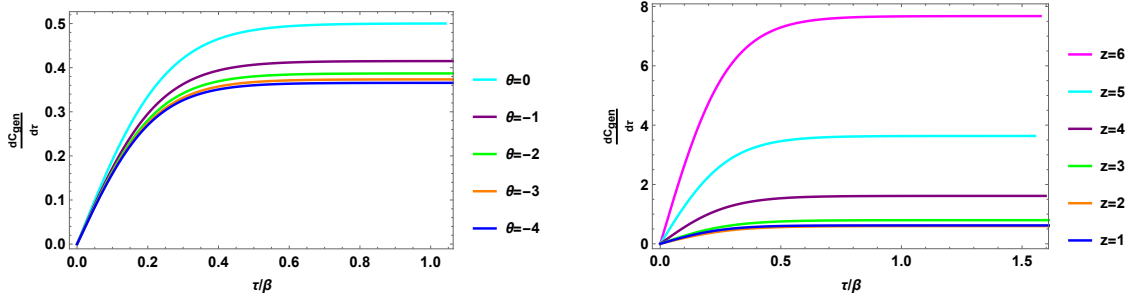


Figure 24. The growth rate $\frac{dC_{\text{gen}}}{d\tau}$ as a function of τ/β for $a(r) = 1 + \lambda_1 R + \lambda_2 R_{\mu\nu} R^{\mu\nu} + \lambda_3 L^4 R_{\mu\nu\rho\sigma} R^{\mu\nu\rho\sigma}$ and different values of d , θ and z : *Left*) $d = 1$, $z = 1$, $\lambda_1 = -10^{-4}$, $\lambda_2 = 10^{-5}$ and $\lambda_3 = -10^{-5}$. *Right*) $d = 2$, $\theta = 1$, $\lambda_1 = -10^{-2}$, $\lambda_2 = -10^{-2}$ and $\lambda_3 = 10^{-2}$.

References

- [1] T. Nishioka, S. Ryu and T. Takayanagi, “Holographic Entanglement Entropy: An Overview,” *J. Phys. A* **42**, 504008 (2009) [arXiv:0905.0932 [hep-th]].
- [2] M. Rangamani and T. Takayanagi, “Holographic Entanglement Entropy,” *Lect. Notes Phys.* **931**, pp.1-246 (2017) [arXiv:1609.01287 [hep-th]].
- [3] L. Susskind, “Three Lectures on Complexity and Black Holes,” [arXiv:1810.11563 [hep-th]].
- [4] S. Aaronson, “The Complexity of Quantum States and Transformations: From Quantum Money to Black Holes,” arXiv:1607.05256 [quant-ph].
- [5] L. Susskind, “Entanglement is not enough,” *Fortsch. Phys.* **64** (2016) 49 [arXiv:1411.0690 [hep-th]].
- [6] L. Susskind, “Computational Complexity and Black Hole Horizons,” [*Fortsch. Phys.* **64**, 24 (2016)] Addendum: *Fortsch. Phys.* **64**, 44 (2016) [arXiv:1403.5695 [hep-th], arXiv:1402.5674 [hep-th]].
- [7] D. Stanford and L. Susskind, “Complexity and Shock Wave Geometries,” *Phys. Rev. D* **90**, no.12, 126007 (2014) [arXiv:1406.2678 [hep-th]].
- [8] A. R. Brown, D. A. Roberts, L. Susskind, B. Swingle and Y. Zhao, “Holographic Complexity Equals Bulk Action?,” *Phys. Rev. Lett.* **116**, no. 19, 191301 (2016) [arXiv:1509.07876 [hep-th]].
- [9] A. R. Brown, D. A. Roberts, L. Susskind, B. Swingle and Y. Zhao, “Complexity, action, and black holes,” *Phys. Rev. D* **93**, no.8, 086006 (2016) [arXiv:1512.04993 [hep-th]].
- [10] J. M. Maldacena, “The Large N limit of superconformal field theories and supergravity,” *Int. J. Theor. Phys.* **38**, 1113-1133 (1999) [arXiv:hep-th/9711200 [hep-th]].
- [11] M. Alishahiha, “Holographic Complexity,” *Phys. Rev. D* **92**, no. 12, 126009 (2015) [arXiv:1509.06614 [hep-th]].
- [12] O. Ben-Ami and D. Carmi, “On Volumes of Subregions in Holography and Complexity,” *JHEP* **11**, 129 (2016) [arXiv:1609.02514 [hep-th]].
- [13] S. Ryu and T. Takayanagi, “Holographic derivation of entanglement entropy from AdS/CFT,” *Phys. Rev. Lett.* **96**, 181602 (2006) [arXiv:hep-th/0603001 [hep-th]].
- [14] V. E. Hubeny, M. Rangamani and T. Takayanagi, “A Covariant holographic entanglement entropy proposal,” *JHEP* **07**, 062 (2007) [arXiv:0705.0016 [hep-th]].
- [15] J. Couch, W. Fischler and P. H. Nguyen, “Noether charge, black hole volume, and complexity,” *JHEP* **1703**, 119 (2017) [arXiv:1610.02038 [hep-th]].
- [16] L. Susskind and Y. Zhao, “Switchbacks and the Bridge to Nowhere,” [arXiv:1408.2823 [hep-th]].
- [17] R. G. Cai, S. M. Ruan, S. J. Wang, R. Q. Yang and R. H. Peng, “Action growth for AdS black holes,” *JHEP* **09**, 161 (2016) [arXiv:1606.08307 [gr-qc]].
- [18] A. R. Brown, L. Susskind and Y. Zhao, “Quantum Complexity and Negative Curvature,” *Phys. Rev. D* **95**, no.4, 045010 (2017) [arXiv:1608.02612 [hep-th]].
- [19] R. G. Cai, M. Sasaki and S. J. Wang, “Action growth of charged black holes with a single horizon,” *Phys. Rev. D* **95**, no.12, 124002 (2017) [arXiv:1702.06766 [gr-qc]].

- [20] M. M. Qaemmaqami, “Complexity growth in minimal massive 3D gravity,” *Phys. Rev. D* **97**, no.2, 026006 (2018) [arXiv:1709.05894 [hep-th]].
- [21] D. Carmi, S. Chapman, H. Marrochio, R. C. Myers and S. Sugishita, “On the Time Dependence of Holographic Complexity,” *JHEP* **11**, 188 (2017) [arXiv:1709.10184 [hep-th]].
- [22] R. Q. Yang, C. Niu, C. Y. Zhang and K. Y. Kim, “Comparison of holographic and field theoretic complexities for time dependent thermofield double states,” *JHEP* **02**, 082 (2018) [arXiv:1710.00600 [hep-th]].
- [23] B. Swingle and Y. Wang, “Holographic Complexity of Einstein-Maxwell-Dilaton Gravity,” *JHEP* **09**, 106 (2018) [arXiv:1712.09826 [hep-th]].
- [24] M. Alishahiha, A. Faraji Astaneh, M. R. Mohammadi Mozaffar and A. Mollabashi, “Complexity Growth with Lifshitz Scaling and Hyperscaling Violation,” *JHEP* **07**, 042 (2018) [arXiv:1802.06740 [hep-th]].
- [25] L. Susskind, “Why do Things Fall?,” [arXiv:1802.01198 [hep-th]].
- [26] A. R. Brown, H. Gharibyan, A. Streicher, L. Susskind, L. Thorlacius and Y. Zhao, “Falling Toward Charged Black Holes,” *Phys. Rev. D* **98**, no.12, 126016 (2018) [arXiv:1804.04156 [hep-th]].
- [27] S. Chapman, H. Marrochio and R. C. Myers, “Holographic complexity in Vaidya spacetimes. Part I,” *JHEP* **06**, 046 (2018) [arXiv:1804.07410 [hep-th]].
- [28] R. Auzzi, S. Baiguera and G. Nardelli, “Volume and complexity for warped AdS black holes,” *JHEP* **06**, 063 (2018) [arXiv:1804.07521 [hep-th]].
- [29] S. Chapman, H. Marrochio and R. C. Myers, “Holographic complexity in Vaidya spacetimes. Part II,” *JHEP* **06**, 114 (2018) [arXiv:1805.07262 [hep-th]].
- [30] R. Auzzi, S. Baiguera, M. Grassi, G. Nardelli and N. Zenoni, “Complexity and action for warped AdS black holes,” *JHEP* **09**, 013 (2018) [arXiv:1806.06216 [hep-th]].
- [31] M. Flory and N. Miekley, “Complexity change under conformal transformations in AdS₃/CFT₂,” *JHEP* **05**, 003 (2019) [arXiv:1806.08376 [hep-th]].
- [32] S. A. Hosseini Mansoori, V. Jahnke, M. M. Qaemmaqami and Y. D. Olivas, “Holographic complexity of anisotropic black branes,” *Phys. Rev. D* **100**, no.4, 046014 (2019) [arXiv:1808.00067 [hep-th]].
- [33] H. Ebrahim, M. Asadi and M. Ali-Akbari, “Evolution of Holographic Complexity Near Critical Point,” *JHEP* **09**, 023 (2019) [arXiv:1811.12002 [hep-th]].
- [34] K. Goto, H. Marrochio, R. C. Myers, L. Queimada and B. Yoshida, “Holographic Complexity Equals Which Action?,” *JHEP* **02**, 160 (2019) [arXiv:1901.00014 [hep-th]].
- [35] M. Flory, “WdW-patches in AdS₃ and complexity change under conformal transformations II,” *JHEP* **05**, 086 (2019) [arXiv:1902.06499 [hep-th]].
- [36] R. Q. Yang, H. S. Jeong, C. Niu and K. Y. Kim, “Complexity of Holographic Superconductors,” *JHEP* **04**, 146 (2019) [arXiv:1902.07586 [hep-th]].
- [37] L. Susskind, “Complexity and Newton’s Laws,” *Front. in Phys.* **8**, 262 (2020) [arXiv:1904.12819 [hep-th]].

- [38] A. Bernamonti, F. Galli, J. Hernandez, R. C. Myers, S. M. Ruan and J. Simón, “First Law of Holographic Complexity,” *Phys. Rev. Lett.* **123**, no.8, 081601 (2019) [arXiv:1903.04511 [hep-th]].
- [39] E. Caceres, S. Chapman, J. D. Couch, J. P. Hernandez, R. C. Myers and S. M. Ruan, “Complexity of Mixed States in QFT and Holography,” *JHEP* **03**, 012 (2020) [arXiv:1909.10557 [hep-th]].
- [40] Y. S. An, R. G. Cai, L. Li and Y. Peng, “Holographic complexity growth in an FLRW universe,” *Phys. Rev. D* **101**, no.4, 046006 (2020) [arXiv:1909.12172 [hep-th]].
- [41] S. S. Hashemi, G. Jafari and A. Naseh, “First law of holographic complexity,” *Phys. Rev. D* **102**, no.10, 106008 (2020) [arXiv:1912.10436 [hep-th]].
- [42] A. Bernamonti, F. Galli, J. Hernandez, R. C. Myers, S. M. Ruan and J. Simón, “Aspects of The First Law of Complexity,” *J. Phys. A* **53**, 29 (2020) [arXiv:2002.05779 [hep-th]].
- [43] L. Susskind and Y. Zhao, “Complexity and Momentum,” *JHEP* **21**, 239 (2020) [arXiv:2006.03019 [hep-th]].
- [44] A. Mounim and W. Mück, “Reparameterization dependence is useful for holographic complexity,” *JHEP* **07**, 010 (2021) [arXiv:2101.10909 [hep-th]].
- [45] D. Ávila, C. Díaz, Y. D. Olivas and L. Patiño, *Phys. Rev. D* **104**, no.6, 066011 (2021) [arXiv:2104.12796 [hep-th]].
- [46] R. Auzzi, S. Baiguera, S. Bonansea, G. Nardelli and K. Toccacelo, “Volume complexity for Janus AdS₃ geometries,” *JHEP* **08**, 045 (2021) [arXiv:2105.08729 [hep-th]].
- [47] S. Baiguera, S. Bonansea and K. Toccacelo, “Volume complexity for the nonsupersymmetric Janus AdS₅ geometry,” *Phys. Rev. D* **104**, no.8, 086030 (2021) [arXiv:2105.12743 [hep-th]].
- [48] A. Belin, R. C. Myers, S. M. Ruan, G. Sárosi and A. J. Speranza, “Does Complexity Equal Anything?,” *Phys. Rev. Lett.* **128**, no.8, 081602 (2022) [arXiv:2111.02429 [hep-th]].
- [49] E. Jørstad, R. C. Myers and S. M. Ruan, “Holographic complexity in dS_{d+1},” *JHEP* **05**, 119 (2022) [arXiv:2202.10684 [hep-th]].
- [50] A. Chowdhury Roy, A. Saha and S. Gangopadhyay, “Mixed state information theoretic measures in boosted black brane,” [arXiv:2204.08012 [hep-th]].
- [51] R. Auzzi, S. Bolognesi, E. Rabinovici, F. I. Schaposnik Massolo and G. Tallarita, “On the time dependence of holographic complexity for charged AdS black holes with scalar hair,” [arXiv:2205.03365 [hep-th]].
- [52] E. Bakshaei, A. Mollabashi and A. Shirzad, “Holographic Subregion Complexity for Singular Surfaces,” *Eur. Phys. J. C* **77**, no.10, 665 (2017) [arXiv:1703.03469 [hep-th]].
- [53] M. Alishahiha and A. Faraji Astaneh, “Holographic Fidelity Susceptibility,” *Phys. Rev. D* **96**, no.8, 086004 (2017) [arXiv:1705.01834 [hep-th]].
- [54] R. Abt, J. Erdmenger, H. Hinrichsen, C. M. Melby-Thompson, R. Meyer, C. Northe and I. A. Reyes, “Topological Complexity in AdS₃/CFT₂,” *Fortsch. Phys.* **66**, no.6, 1800034 (2018) [arXiv:1710.01327 [hep-th]].
- [55] B. Chen, W. M. Li, R. Q. Yang, C. Y. Zhang and S. J. Zhang, “Holographic subregion complexity under a thermal quench,” *JHEP* **07**, 034 (2018) [arXiv:1803.06680 [hep-th]].

- [56] C. A. Agón, M. Headrick and B. Swingle, “Subsystem Complexity and Holography,” *JHEP* **02**, 145 (2019) [arXiv:1804.01561 [hep-th]].
- [57] R. Abt, J. Erdmenger, M. Gerbershagen, C. M. Melby-Thompson and C. Northe, “Holographic Subregion Complexity from Kinematic Space,” *JHEP* **01**, 012 (2019) [arXiv:1805.10298 [hep-th]].
- [58] M. Alishahiha, K. Babaei Velni and M. R. Mohammadi Mozaffar, “Black hole subregion action and complexity,” *Phys. Rev. D* **99**, no.12, 126016 (2019) [arXiv:1809.06031 [hep-th]].
- [59] R. Auzzi, S. Baiguera, A. Mitra, G. Nardelli and N. Zenoni, “Subsystem complexity in warped AdS,” *JHEP* **09**, 114 (2019) [arXiv:1906.09345 [hep-th]].
- [60] R. Auzzi, G. Nardelli, F. I. Schaposnik Massolo, G. Tallarita and N. Zenoni, “On volume subregion complexity in Vaidya spacetime,” *JHEP* **11**, 098 (2019) [arXiv:1908.10832 [hep-th]].
- [61] R. Auzzi, S. Baiguera, A. Legramandi, G. Nardelli, P. Roy and N. Zenoni, “On subregion action complexity in AdS₃ and in the BTZ black hole,” *JHEP* **01**, 066 (2020) [arXiv:1910.00526 [hep-th]].
- [62] P. Braccia, A. L. Cotrone and E. Tonni, “Complexity in the presence of a boundary,” *JHEP* **02**, 051 (2020) [arXiv:1910.03489 [hep-th]].
- [63] Z. Borvayeh, M. R. Tanhayi and S. Rafibakhsh, “Holographic Complexity of Subregions in the Hyperscaling Violating Theories,” *Mod. Phys. Lett. A* **35**, no.23, 2050191 (2020) [arXiv:2006.08478 [hep-th]].
- [64] A. Bhattacharya, A. Bhattacharyya, P. Nandy and A. K. Patra, “Partial islands and subregion complexity in geometric secret-sharing model,” *JHEP* **12**, 091 (2021) [arXiv:2109.07842 [hep-th]].
- [65] A. Bhattacharya, A. Bhattacharyya, P. Nandy and A. K. Patra, “Islands and complexity of eternal black hole and radiation subsystems for a doubly holographic model,” *JHEP* **05**, 135 (2021) [arXiv:2103.15852 [hep-th]].
- [66] R. Auzzi, S. Baiguera, S. Bonansea and G. Nardelli, “Action complexity in the presence of defects and boundaries,” *JHEP* **02**, 118 (2022) [arXiv:2112.03290 [hep-th]].
- [67] A. Bhattacharya, A. Bhattacharyya, P. Nandy and A. K. Patra, “Bath deformations, islands, and holographic complexity,” *Phys. Rev. D* **105**, no.6, 066019 (2022) [arXiv:2112.06967 [hep-th]].
- [68] S. Chapman, H. Marrochio and R. C. Myers, “Complexity of Formation in Holography,” *JHEP* **01**, 062 (2017) [arXiv:1610.08063 [hep-th]].
- [69] A. Bernamonti, F. Bigazzi, D. Billo, L. Faggi and F. Galli, “Holographic and QFT complexity with angular momentum,” *JHEP* **11**, 037 (2021) [arXiv:2108.09281 [hep-th]].
- [70] A. Akhavan and F. Omidi, “On the Role of Counterterms in Holographic Complexity,” *JHEP* **11**, 054 (2019) [arXiv:1906.09561 [hep-th]].
- [71] A. R. Brown, H. Gharibyan, H. W. Lin, L. Susskind, L. Thorlacius and Y. Zhao, “Complexity of Jackiw-Teitelboim gravity,” *Phys. Rev. D* **99**, no.4, 046016 (2019) [arXiv:1810.08741 [hep-th]].
- [72] M. Alishahiha, “On complexity of Jackiw–Teitelboim gravity,” *Eur. Phys. J. C* **79**, no.4, 365 (2019) [arXiv:1811.09028 [hep-th]].

- [73] M. Alishahiha, S. Banerjee and J. Kames-King, “Complexity via Replica Trick,” [arXiv:2205.01150 [hep-th]].
- [74] M. Alishahiha, A. Faraji Astaneh, A. Naseh and M. H. Vahidinia, “On complexity for F(R) and critical gravity,” JHEP **05**, 009 (2017) [arXiv:1702.06796 [hep-th]].
- [75] Y. S. An, R. G. Cai and Y. Peng, “Time Dependence of Holographic Complexity in Gauss-Bonnet Gravity,” Phys. Rev. D **98**, no.10, 106013 (2018) [arXiv:1805.07775 [hep-th]].
- [76] T. Mandal, A. Mitra and G. S. Punia, “Action complexity of charged black holes with higher derivative interactions,” [arXiv:2205.11201 [hep-th]].
- [77] A. Mounim and W. Mück, “Reparametrization dependence and holographic complexity of black holes,” Phys. Rev. D **105**, no.2, 026024 (2022) [arXiv:2106.01897 [hep-th]].
- [78] A. Akhavan, M. Alishahiha, A. Naseh and H. Zolfi, “Complexity and Behind the Horizon Cut Off,” JHEP **12**, 090 (2018) [arXiv:1810.12015 [hep-th]].
- [79] M. Alishahiha, K. Babaei Velni and M. Reza Tanhayi, “Complexity and near extremal charged black branes,” Annals Phys. **425**, 168398 (2021) [arXiv:1901.00689 [hep-th]].
- [80] S. S. Hashemi, G. Jafari, A. Naseh and H. Zolfi, “More on Complexity in Finite Cut Off Geometry,” Phys. Lett. B **797**, 134898 (2019) [arXiv:1902.03554 [hep-th]].
- [81] M. Alishahiha and A. Faraji Astaneh, “Complexity of Holographic Theories at Finite Cutoff,” Phys. Rev. D **100**, no.8, 086004 (2019) [arXiv:1905.10740 [hep-th]].
- [82] M. Alishahiha, S. Banerjee, J. Kames-King and E. Loos, “Complexity as a holographic probe of strong cosmic censorship,” Phys. Rev. D **105**, no.2, 026001 (2022) [arXiv:2106.14578 [hep-th]].
- [83] D. Carmi, R. C. Myers and P. Rath, “Comments on Holographic Complexity,” JHEP **1703**, 118 (2017) [arXiv:1612.00433 [hep-th]].
- [84] A. Reynolds and S. F. Ross, “Divergences in Holographic Complexity,” Class. Quant. Grav. **34**, no. 10, 105004 (2017) [arXiv:1612.05439 [hep-th]].
- [85] F. Omidi, “Regularizations of Action-Complexity for a Pure BTZ Black Hole Microstate,” JHEP **07**, 020 (2020) [arXiv:2004.11628 [hep-th]].
- [86] L. Lehner, R. C. Myers, E. Poisson and R. D. Sorkin, “Gravitational action with null boundaries,” Phys. Rev. D **94**, no.8, 084046 (2016) [arXiv:1609.00207 [hep-th]].
- [87] R. Q. Yang, C. Niu and K. Y. Kim, “Surface Counterterms and Regularized Holographic Complexity,” JHEP **09**, 042 (2017) [arXiv:1701.03706 [hep-th]].
- [88] A. R. Brown and L. Susskind, “Second law of quantum complexity,” Phys. Rev. D **97**, no.8, 086015 (2018) [arXiv:1701.01107 [hep-th]].
- [89] R. Jefferson and R. C. Myers, “Circuit complexity in quantum field theory,” JHEP **1710**, 107 (2017) [arXiv:1707.08570 [hep-th]].
- [90] S. Chapman, M. P. Heller, H. Marrochio and F. Pastawski, “Toward a Definition of Complexity for Quantum Field Theory States,” Phys. Rev. Lett. **120**, no. 12, 121602 (2018) [arXiv:1707.08582 [hep-th]].
- [91] R. Khan, C. Krishnan and S. Sharma, “Circuit Complexity in Fermionic Field Theory,” Phys. Rev. D **98**, no.12, 126001 (2018) [arXiv:1801.07620 [hep-th]].

- [92] L. Hackl and R. C. Myers, “Circuit complexity for free fermions,” *JHEP* **1807**, 139 (2018) [arXiv:1803.10638 [hep-th]].
- [93] H. A. Camargo, P. Caputa, D. Das, M. P. Heller and R. Jefferson, “Complexity as a novel probe of quantum quenches: universal scalings and purifications,” *Phys. Rev. Lett.* **122**, no.8, 081601 (2019) [arXiv:1807.07075 [hep-th]].
- [94] M. Guo, J. Hernandez, R. C. Myers and S. M. Ruan, “Circuit Complexity for Coherent States,” *JHEP* **10**, 011 (2018) [arXiv:1807.07677 [hep-th]].
- [95] R. Q. Yang, Y. S. An, C. Niu, C. Y. Zhang and K. Y. Kim, “More on complexity of operators in quantum field theory,” *JHEP* **03**, 161 (2019) [arXiv:1809.06678 [hep-th]].
- [96] T. Ali, A. Bhattacharyya, S. Shajidul Haque, E. H. Kim and N. Moynihan, “Time Evolution of Complexity: A Critique of Three Methods,” *JHEP* **04**, 087 (2019) [arXiv:1810.02734 [hep-th]].
- [97] S. Chapman, J. Eisert, L. Hackl, M. P. Heller, R. Jefferson, H. Marrochio and R. C. Myers, “Complexity and entanglement for thermofield double states,” *SciPost Phys.* **6**, no. 3, 034 (2019) [arXiv:1810.05151 [hep-th]].
- [98] R. Q. Yang and K. Y. Kim, “Complexity of operators generated by quantum mechanical Hamiltonians,” *JHEP* **03**, 010 (2019) [arXiv:1810.09405 [hep-th]].
- [99] A. R. Brown and L. Susskind, “Complexity geometry of a single qubit,” *Phys. Rev. D* **100**, no.4, 046020 (2019) [arXiv:1903.12621 [hep-th]].
- [100] H. A. Camargo, M. P. Heller, R. Jefferson and J. Knaute, “Path integral optimization as circuit complexity,” *Phys. Rev. Lett.* **123**, no.1, 011601 (2019) [arXiv:1904.02713 [hep-th]].
- [101] T. Ali, A. Bhattacharyya, S. S. Haque, E. H. Kim, N. Moynihan and J. Murugan, “Chaos and Complexity in Quantum Mechanics,” *Phys. Rev. D* **101**, no.2, 026021 (2020) [arXiv:1905.13534 [hep-th]].
- [102] R. Q. Yang and K. Y. Kim, “Time evolution of the complexity in chaotic systems: a concrete example,” *JHEP* **05**, 045 (2020) [arXiv:1906.02052 [hep-th]].
- [103] A. Bhattacharyya, P. Nandy and A. Sinha, “Renormalized Circuit Complexity,” *Phys. Rev. Lett.* **124**, no.10, 101602 (2020) [arXiv:1907.08223 [hep-th]].
- [104] A. Bhattacharyya, W. Chemissany, S. Shajidul Haque and B. Yan, “Towards the web of quantum chaos diagnostics,” *Eur. Phys. J. C* **82**, no.1, 87 (2022) [arXiv:1909.01894 [hep-th]].
- [105] A. Bhattacharyya, S. Das, S. Shajidul Haque and B. Underwood, “Cosmological Complexity,” *Phys. Rev. D* **101**, no.10, 106020 (2020) [arXiv:2001.08664 [hep-th]].
- [106] M. Doroudiani, A. Naseh and R. Pirmoradian, “Complexity for Charged Thermofield Double States,” *JHEP* **01**, 120 (2020) [arXiv:1910.08806 [hep-th]].
- [107] M. Flory and M. P. Heller, “Geometry of Complexity in Conformal Field Theory,” *Phys. Rev. Res.* **2**, no.4, 043438 (2020) [arXiv:2005.02415 [hep-th]].
- [108] A. Bhattacharyya, S. Das, S. S. Haque and B. Underwood, “Rise of cosmological complexity: Saturation of growth and chaos,” *Phys. Rev. Res.* **2**, no.3, 033273 (2020) [arXiv:2005.10854 [hep-th]].
- [109] G. Di Giulio and E. Tonni, “Complexity of mixed Gaussian states from Fisher information geometry,” *JHEP* **12**, 101 (2020) [arXiv:2006.00921 [hep-th]].

- [110] A. Bhattacharyya, W. Chemissany, S. S. Haque, J. Murugan and B. Yan, “The Multi-faceted Inverted Harmonic Oscillator: Chaos and Complexity,” *SciPost Phys. Core* **4**, 002 (2021) [arXiv:2007.01232 [hep-th]].
- [111] M. Flory and M. P. Heller, “Conformal field theory complexity from Euler-Arnold equations,” *JHEP* **12**, 091 (2020) [arXiv:2007.11555 [hep-th]].
- [112] H. A. Camargo, L. Hackl, M. P. Heller, A. Jahn, T. Takayanagi and B. Windt, *Phys. Rev. Res.* **3**, no.1, 013248 (2021) [arXiv:2009.11881 [hep-th]].
- [113] R. Auzzi, S. Baiguera, G. B. De Luca, A. Legramandi, G. Nardelli and N. Zenoni, “Geometry of quantum complexity,” *Phys. Rev. D* **103**, no.10, 106021 (2021) [arXiv:2011.07601 [hep-th]].
- [114] A. Bhattacharyya, S. S. Haque and E. H. Kim, “Complexity from the reduced density matrix: a new diagnostic for chaos,” *JHEP* **10**, 028 (2021) [arXiv:2011.04705 [hep-th]].
- [115] R. Q. Yang, Y. S. An, C. Niu, C. Y. Zhang and K. Y. Kim, “What kind of “complexity” is dual to holographic complexity?,” *Eur. Phys. J. C* **82**, no.3, 262 (2022) [arXiv:2011.14636 [hep-th]].
- [116] G. Di Giulio and E. Tonni, “Subsystem complexity after a global quantum quench,” *JHEP* **05**, 022 (2021) [arXiv:2102.02764 [hep-th]].
- [117] N. Chagnet, S. Chapman, J. de Boer and C. Zukowski, “Complexity for Conformal Field Theories in General Dimensions,” *Phys. Rev. Lett.* **128**, no.5, 051601 (2022) [arXiv:2103.06920 [hep-th]].
- [118] S. S. Haque, C. Jana and B. Underwood, “Saturation of thermal complexity of purification,” *JHEP* **01**, 159 (2022) [arXiv:2107.08969 [hep-th]].
- [119] A. Moghimnejad and S. Parvizi, “Circuit complexity in U(1) gauge theory,” *Mod. Phys. Lett. A* **36**, no.34, 2150240 (2021) [arXiv:2108.08208 [hep-th]].
- [120] P. Basteiro, J. Erdmenger, P. Fries, F. Goth, I. Matthaikakakis and R. Meyer, “Quantum Complexity as Hydrodynamics,” [arXiv:2109.01152 [hep-th]].
- [121] S. S. Haque, C. Jana and B. Underwood, “Operator Complexity for Continuous Variable Systems,” [arXiv:2110.08356 [hep-th]].
- [122] A. R. Brown, M. H. Freedman, H. W. Lin and L. Susskind, “Effective Geometry, Complexity, and Universality,” [arXiv:2111.12700 [hep-th]].
- [123] A. Bhattacharyya, T. Hanif, S. S. Haque and M. K. Rahman, “Complexity for an open quantum system,” *Phys. Rev. D* **105**, no.4, 046011 (2022) [arXiv:2112.03955 [hep-th]].
- [124] A. R. Brown, “A Quantum Complexity Lowerbound from Differential Geometry,” [arXiv:2112.05724 [hep-th]].
- [125] J. Erdmenger, M. Flory, M. Gerbershagen, M. P. Heller and A. L. Weigel, “Exact Gravity Duals for Simple Quantum Circuits,” [arXiv:2112.12158 [hep-th]].
- [126] A. R. Brown, “Polynomial Equivalence of Complexity Geometries,” [arXiv:2205.04485 [quant-ph]].
- [127] M. Alishahiha, E. O Colgain and H. Yavartanoo, “Charged Black Branes with Holographic Complexity Violating Factor,” *JHEP* **11**, 137 (2012) [arXiv:1209.3946 [hep-th]].

- [128] F. Omidi, “Entropy of Hawking radiation for two-sided hyperscaling violating black branes,” *JHEP* **04**, 022 (2022) [arXiv:2112.05890 [hep-th]].
- [129] X. Dong, S. Harrison, S. Kachru, G. Torroba and H. Wang, “Aspects of holography for theories with hyperscaling violation,” *JHEP* **06**, 041 (2012) [arXiv:1201.1905 [hep-th]].
- [130] J. F. Pedraza, W. Sybesma and M. R. Visser, “Hyperscaling violating black holes with spherical and hyperbolic horizons,” *Class. Quant. Grav.* **36**, no.5, 054002 (2019) [arXiv:1807.09770 [hep-th]].
- [131] E. Shaghoulian, “Holographic Entanglement Entropy and Fermi Surfaces,” *JHEP* **05**, 065 (2012) [arXiv:1112.2702 [hep-th]].
- [132] C. Charmousis, B. Gouteraux, B. S. Kim, E. Kiritsis and R. Meyer, “Effective Holographic Theories for low-temperature condensed matter systems,” *JHEP* **11**, 151 (2010) [arXiv:1005.4690 [hep-th]].
- [133] R. Emparan, C. V. Johnson and R. C. Myers, “Surface terms as counterterms in the AdS / CFT correspondence,” *Phys. Rev. D* **60**, 104001 (1999) [arXiv:hep-th/9903238 [hep-th]].